Premature upregulation of miR-92a's target RBFOX2 hijacks PTBP splicing and impairs cortical neuronal differentiation.

Stephan Weißbach[1,2], Hristo Todorov[2,3], Laura Schlichtholz[2], Sophia Mühlbauer[2], Lea Zografidou[2], Azza Soliman[2], Sarah Lor-Zade[2], Dewi Hartwich[2], Dennis Strand[4], Susanne Strand[4], Tanja Vogel[5], Martin Heine[1], Susanne Gerber[2], Jennifer Winter[2,*]

[1] Institute of Developmental Biology and Neurobiology (iDN), Johannes Gutenberg-University, 55128 Mainz, Germany

[2] Institute of Human Genetics, University Medical Center, Johannes Gutenberg-University, 55131 Mainz, Germany

[3] Current affiliation: Institute of Immunology, University Medical Center, Johannes Gutenberg-University, 55131 Mainz, Germany

[4] Department of Internal Medicine, University Medical Center, Johannes Gutenberg-University, 55131 Mainz, Germany

[5] Institute of Anatomy and Cell Biology, Department of Molecular Embryology, Medical Faculty, Albert-Ludwigs-University Freiburg, 79104 Freiburg, Germany

[*] Corresponding author: jewinter@uni-mainz.de

Abstract

RBFOX2 is an RNA-binding protein crucial for alternative splicing regulation and implicated in several neurodevelopmental disorders. Here, we show that while RBFOX2 is present only at low levels in neural progenitor cells (NPCs), it is upregulated in differentiating neurons of the mouse embryonic neocortex. *In-utero*-electroporation-induced overexpression resulted in a cellular phenotype characterized by impaired neuronal migration and differentiation. Genome-wide analysis at E15.5 revealed numerous alternative splicing events associated with a mixed NPC- and neuron-like splicing pattern and a significant deviation from the normal splicing developmental trajectory. Remarkably, premature *Rbfox2* overexpression induced the inclusion of validated target exons that are otherwise repressed by PTBP2, indicating an antagonistic splicing relationship between these two RNA-binding proteins and highlighting the necessity for strict temporal regulation of their expression during embryonic brain development. Consequently, we showed that the NPC-specific miRNA 92a-3p reduced the expression levels of *Rbfox2 in vitro*. Furthermore, silencing miR-92a-3p *in vivo* in the embryonic neocortex led to a significant increase in *Rbfox2* levels. Our results therefore demonstrate that RBFOX2 is a crucial player in the NPC-to-neuron splicing switch. Furthermore, we present a novel post-transcriptional mechanism for controlling RBFOX2 levels during early neuronal differentiation via miR-92a-3p silencing.

Introduction

Despite the presence of only approximately 22,000 protein-coding genes[1], the murine neocortex, and hippocampus exhibit a considerable diversity of neurons, amounting to 388 transcriptomic cell types, as reported by the Allen Brain Consortium[2]. A key factor enabling this diversity and complexity is alternative splicing (AS), a tightly regulated process that governs the production of multiple mRNA isoforms from a single gene. Intriguingly, nearly every multi-exon gene in the human genome can undergo alternative splicing, generating numerous protein isoforms with distinct structural and

functional properties[3]. This vast molecular diversity expands the proteome's complexity without necessitating a proportional increase in the genome's size. Within the nervous system, AS is a pervasive phenomenon, with various neural genes subject to this regulation[4]. Overall, AS has a higher prevalence across different species and is more conserved in the brain compared to other tissues[5,6].

Specifically, numerous changes in the splicing landscape occur in the developing brain with high temporal precision[4,7]. Among the processes that require correct splicing are neuronal migration, neuronal differentiation[8], axonogenesis[9], and synaptogenesis[10,11]. Notably, the significance of correct splicing is not confined to the developing brain alone. In the adult brain, different neuronal types exhibit distinct splicing patterns, further underscoring the importance of alternative splicing in maintaining the brain's functional diversity[11,12].

During embryonic development, neural stem cell differentiation requires precise extensive AS switches to create neuron-specific splicing patterns. Many of these splicing events alter key protein domains, particularly in proteins of the cytoskeleton[8]. Various RNA binding proteins (RBPs) regulate the transition from neural stem and progenitor cells to neurons by altering the splicing pattern of target genes, therefore their temporal expression needs to be strictly regulated. Here, microRNAs (miRNAs) that suppress gene expression post-transcriptionally by binding to the 3' untranslated region of target mRNAs[13–16], represent one important mechanism for mediating stage and cell-type specific levels of RBPs For instance, PTBP1 is expressed only in neural stem and progenitor cells, however, it is strongly repressed by miR-124-3p in neurons[17]. In contrast, other prominent RBPs, including NOVA, PTBP2, MBNL2, and RBFOX are predominant in neurons. These RBPs act in both synergistic (e.g. NOVA and RBFOX) and antagonistic relationships (e.g. PTBP1/2 and RBFOX)[18,4,8].

The RBFOX-family consists of three paralogs, namely, RBFOX1 (FOX-1 or A2B1), RBFOX2 (FOX-2 or RBM9) and RBFOX3 (FOX-3, HRNBP3, or NeuN). The association of mutations in human *RBFOX1* and *RBFOX2* with intellectual disability, autism, and other neurodevelopmental disorders, as well as the specific neurological phenotypes observed in *Rbfox* knockout mice, highlight the important functions of these proteins during neurodevelopment[19–26]. All RBFOX-proteins have a single, highly conserved RNA recognition motif (RRM) that binds to the target sequence (U)GCAUG harbored in the premature mRNA and initiates position-dependent splicing. RBFOX binding in the intronic region upstream of an alternatively spliced exon promotes its exclusion from the mature mRNA whereas downstream binding leads to inclusion[27]. Moreover, in humans, all RBFOX-proteins share the position-dependent splicing mechanism and the RRM which is identical in RBFOX1 and RBFOX2 and almost identical in RBFOX3. Therefore, the RBFOX family can act in a functionally redundant manner[28]. However, the temporal expression patterns of these proteins diverge significantly, exhibiting variations across different tissues and cell types[2,12]. In the developing brain, RBFOX proteins are either lowly expressed or not present in neural stem cells, but they are highly expressed in neurons which is in agreement with their role in promoting neuronal differentiation. Studies aiming at identifying splicing changes during neural stem cell differentiation have compared alternative exon usage between NPCs and neurons by RNA-sequencing[8,29]. While these studies have identified numerous splicing changes that are presumably driven by RBFOX binding, the exact role of RBFOX during neuronal differentiation in the embryonic brain has not been elucidated yet.

In the current study, we identified extensive AS changes upon premature *Rbfox2* overexpression (*Rbfox2*-OE) in the embryonic neocortex, specifically related to genes that are important for neuronal differentiation and localization. Remarkably, we observed a mixed neuronal and NPC-like splicing pattern that significantly deviated from the normal cortical splicing trajectory. In line with this, *Rbfox2* overexpression increased the percentage of neural stem and progenitor cells and blocked differentiation into neurons on the cellular level. Since a precise and tight control of RBFOX2 is essential for proper neuronal differentiation in the embryonic neocortex, we investigated if miRNAs might repress *Rbfox2* expression in NPCs. Indeed, we observed that the NPC-specific miR-92a led to reduced RBFOX2 levels. Conversely, miR-92a silencing in the embryonic neocortex was associated with a concomitant increase in *Rbfox2* expression.

Results

RBFOX2 is predominantly expressed in neurons

The RBFOX protein family exhibits distinct temporal expression patterns, varying also by cell type. For instance, RBFOX1 and RBFOX3 are expressed in mature neurons and exclusively in the cortical plate in the embryonic cerebral cortex[30] RBFOX2 shows early expression in Purkinje cells in the cerebellum[31]. To elucidate the composition of RBFOX proteins in the mouse embryonic cerebral cortex, we co-stained sections for RBFOX1 and RBFOX2. This confirmed RBFOX2's presence was not limited to the neuron-specific cortical plate, but it was also expressed in the intermediate and ventricular (VZ)/subventricular (SVZ) zones (Figure 1a). In contrast, RBFOX1 expression was restricted to the cortical plate/subplate. While this broader expression pattern of RBFOX2 compared to RBFOX1 was evident, not all cells in the cerebral cortex showed positive RBFOX2 staining. Especially in the VZ/SVZ where radial glia cells and basal progenitors reside at this developmental stage, the majority of cells were RBFOX2 negative (Figure 1a). This prompted us to investigate the temporal expression of RBFOX2 using an *in vitro* neuronal differentiation model. Here, we observed low *Rbfox2* mRNA expression in radial glia-like cells and early neural progenitor cells (NPCs). However, *Rbfox2* expression increased significantly during neuronal differentiation, peaking in late NPCs and young neurons (Figure 1b). Likewise, *Rbfox2* was only weakly expressed in NPCs derived from the embryonic cerebral cortex while it was strongly upregulated in cortical neurons at both RNA and protein levels (Figure 1c, d).

To further corroborate these data, we analyzed RBFOX2 expression in the embryonic cerebral cortex *in vivo* by immunostaining. To this end, we made use of a transgenic mouse model (HES5::GFP) expressing GFP exclusively in Notch-signaling neural progenitor cells. In agreement with the *in vitro* data, RBFOX2 expression was restricted to GFP^{-} cells, that were presumably in a more differentiated state compared to HES5 positive NPCs (Figure 1e). Co-stainings with the basal progenitor marker TBR2 (EOMES) confirmed the absence of RBFOX2 from neural progenitor cells. Only cells with a low TBR2 expression exhibited low RBFOX2 expression, suggesting that these cells were currently differentiating into neurons (Figure 1f). In contrast, RBFOX2 was highly expressed in newborn neurons in all zones as revealed by co-staining with the early neuron marker β-III-Tubulin (TUBB3) (Figure 1g). In summary, RBFOX2 was weakly expressed in neural stem and progenitor cells and highly upregulated during neuronal differentiation, highlighting its potential role in mediating the neuron-specific splicing switch.

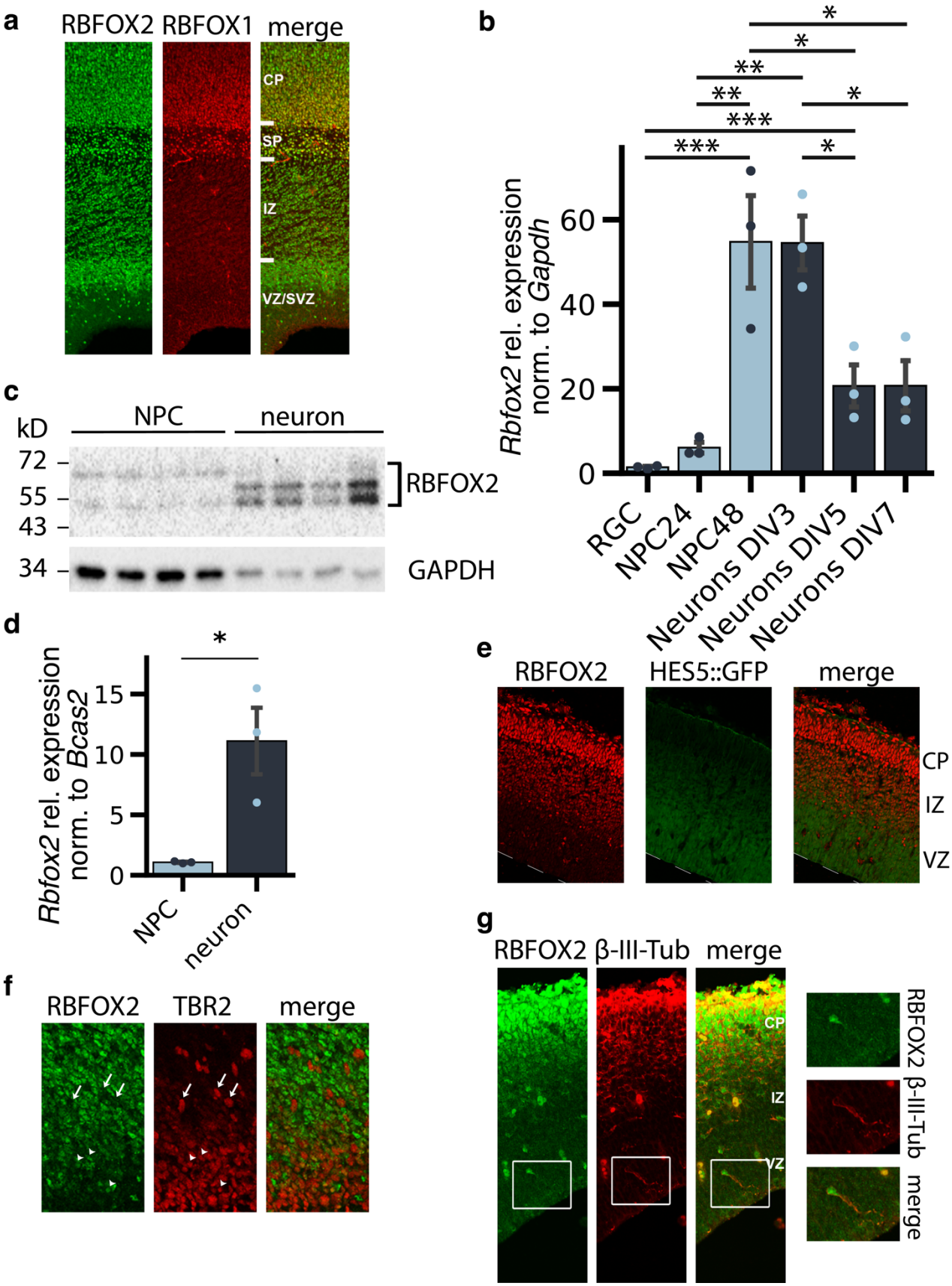

Figure 1 Rbfox2 expression was upregulated in newborn neurons. a) Cryosections of E17.5 cerebral cortex were co-stained with antibodies against RBFOX1 and RBFOX2. Expression of RBFOX1 was restricted to the cortical plate/subplate whereas RBFOX2 was additionally expressed in cells of the ventricular zone (VZ)/subventricular zone (SVZ) and intermediate zone (IZ). b) To determine the expression of Rbfox2 during neuronal differentiation, embryonic stem cells were differentiated into radial glia cells (RGCs), NPCs, and neurons and subjected to RT-qPCR with Rbfox2-specific primers. Rbfox2 expression increased strongly in late NPCs and early neurons and

*decreased again in late neurons. c) Western blot analysis with RBFOX2-specific antibodies illustrates the increase in RBFOX2 expression in neurons compared to NPCs. Note that due to alternative splicing, several RBFOX2 isoforms exist which differ between NPCs and neurons. d) RT-qPCR showed increased Rbfox2 expression in neurons compared to NPCs. e) Cryosections of the E14.5 cerebral cortex derived from HES5::GFP transgenic mice were immunostained with RBFOX2 antibodies. RBFOX2 was predominantly expressed in differentiating GFP^{-} cells. f and g) Cryosections of the E17.5 cerebral cortex were co-immunostained for RBFOX2 and the basal progenitor marker TBR2 (f) or RBFOX2 and the newborn-neuron marker β-III-Tubulin (g). RBFOX2 was expressed in β-III-Tubulin+ neurons and absent from $TBR2^{+}$ basal progenitors. *$p<0.05$, **$p<0.01$, ***$p<0.001$, ANOVA followed by Tukey's post-hoc test in b, t-test in d.*

Premature *Rbfox2* overexpression disrupts the splicing landscape of the developing cortex

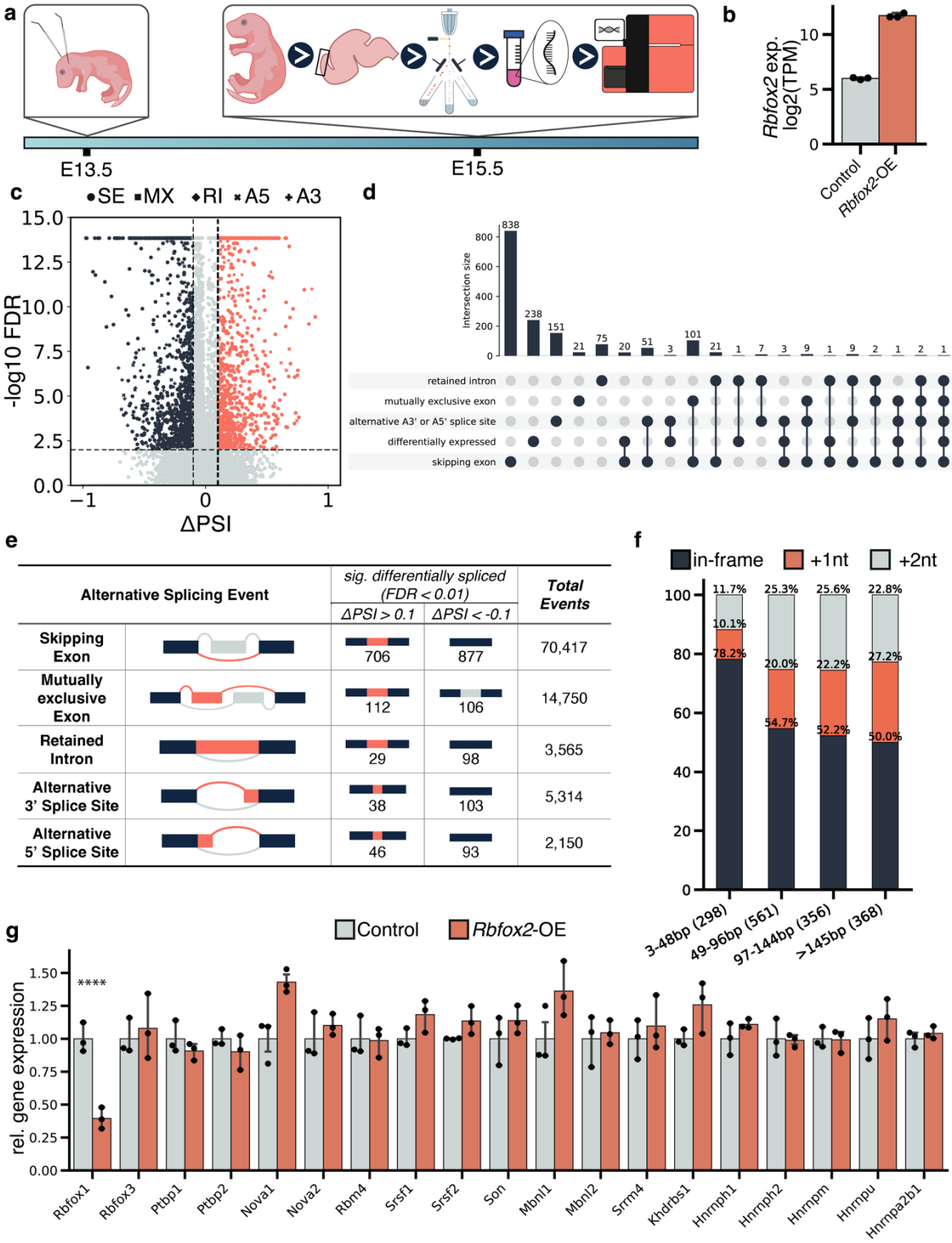

Figure 2 Rbfox2 overexpression changed the splicing pattern of the developing cortex. a) Experimental timeline, Rbfox2 overexpression was induced in embryonic mouse neocortex at E13.5 by in-utero electroporation, and bulk RNA-sequencing was performed at E15.5 b) The electroporation of Rbfox2 constructs increased the mRNA abundance of Rbfox2 in the cortex significantly c) The volcano plot visualizes alternative splicing events. The x-axis shows delta percentage spliced in (ΔPSI), and the y-axis shows -log10 false discovery rate (FDR) values. Significantly spliced-in events are in orange, spliced-out events are in blue, and non-significant events are in grey. Shapes denote event types: circles for skipping exons, squares for mutually exclusive exons (MX), diamonds for retained introns (RI), and crosses for alternative A5 and A3 splice sites. d) UpSet plot depicts the overlap between 1) Differentially expressed genes, 2) Genes with significant alternatively spliced skipping exon events, 3) Genes

*with significant alternatively spliced mutually exclusive exon events, and 4) Genes with other splice events, including retained intron, A3', and A5' splice sites. e) The table provides an overview of significant alternative splicing events, totaling 2,208 events. Significance was defined as FDR < 0.01 and either ΔPSI > 0.1 or ΔPSI < -0.1. f) Frequency of induced frameshifts due to alternative splicing for different exon lengths. g) Normalized gene expression levels of key splicing factors important in the CNS, upon Rbfox2 overexpression compared to control. Values for each gene are normalized to the mean of the control group. Data are shown as mean ± standard error of the mean *** p<0.001, ****p<0.0001, Wald test from DESeq2 in g.*

To study RBFOX2's impact on splicing during embryonic corticogenesis, we used *in-utero* electroporation to overexpress *Rbfox2* in the mouse cerebral cortex at E13.5 and subsequently performed RNA-sequencing at E15.5 (Figure 2a). As expected, *in utero* electroporation resulted in a significant increase in *Rbfox2* gene expression (p_{adj} < 0.0001, log2fold = 5.754, Figure 2b). Furthermore, we detected 268 differentially expressed genes (Supplementary Figure S1a, Supplementary Data 1) and substantial changes in the alternative splicing landscape upon *Rbfox2* overexpression compared to control samples (Figure 2c). However, most alternatively spliced genes did not show altered expression levels. Only 30 genes were alternatively spliced and differentially expressed at the same time (Figure 2d) with *Snhg5*, a lncRNA, having all five types of analyzed splicing events. 17 genes were alternatively spliced and upregulated, while the remaining 13 were downregulated. While frameshifts induced by alternative splicing can result in early stop codons and nonsense-mediated decay (Figure 2f), we did not find significant changes in gene expression related to this phenomenon in our data.

Overall, we detected 2,208 significant alternative splicing events (Figure 2e, Supplementary Figure S2) between the *Rbfox2*-OE and control samples using a stringent threshold of FDR < 0.01 and |ΔPSI| > 0.1. Skipped exons (or cassette exons) represented ~71% of these events. Changes in splicing could mostly be attributed directly to RBFOX2 and not to altered expression of other known splice factors relevant during cortical development (Figure 2g). In line with this, we observed a significant overlap between skipping exon events in our data with *Rbfox* triple knock-out (t*Rbfox*-KO) samples[32] (fold enrichment ≈ 9.833, p-value < 0.0001; Supplementary Figure 3b, Supplementary Data 2). Importantly, inclusion levels of cassette exons present in both data sets were strongly negatively correlated (R = -0.6624, p < 0.0001) indicating that *Rbfox2*-OE induced the opposite splicing regulation compared to t*Rbfox*-KO. (Supplementary Figure 3a). The strong *Rbfox2*-OE induced a significant reduction in the expression level of *Rbfox1* (p_{adj} < 0.0001, log2fold = -1.342). However, the expression of *Rbfox3* was unaltered (p_{adj} ≈ 0.98, log2fold = 0.121) compared to the control group. Remarkably, genes that were alternatively spliced in our analysis were significantly enriched for high-confidence neurodevelopmental disorder (NDD) genes[33] (224 out of 1317 genes, fold enrichment ≈ 1.358, p < 2e-07, Supplementary Data 6, Supplementary Figure S4).

Alternative splicing is a key mediator for the development of proper neuronal functioning. Over 20,000 splicing events have been reported throughout cortical development[34]. To gain a perspective on the splicing pattern induced upon *Rbfox2*-OE, we integrated the previously published RNA-sequencing data from Weyn-Vanhentenryck et al. obtained at different developmental stages of wildtype mouse cerebral cortex (E14.5 to P30)[34] as well as RNA-sequencing from FACS-sorted NPCs and neurons[29]. The hierarchical clustering of splicing events that were significant both in our data and in the previous studies, revealed that our control group clustered with the FACS-sorted neurons as well as with the E14.5 and E16.5 cortical samples. In contrast, the *Rbfox2*-OE group did not closely cluster with any of the embryonic

223 samples or NPCs/neurons pointing to an abnormal splicing pattern (Supplementary
224 Figure S2).
225 To further investigate the impact of *Rbfox2*-OE on the splicing landscape during
226 neurogenesis, we applied a principal component analysis (PCA). We observed a bell-
227 shaped trajectory indicative of the expected splicing changes throughout embryonic
228 and postnatal cortical development (Figure 3a). Remarkably, the influence of batch
229 effects between the different studies was negligible, contrary to differential gene
230 expression analyses where batch effects are often prominent[35,36]. *Rbfox2*-OE resulted
231 in a substantial deviation from this expected developmental trajectory. Specifically, on
232 the first principal component (PC1), *Rbfox2*-OE exhibited a shift towards the splicing
233 pattern associated with mature neurons, while on the second principal component
234 (PC2), the shift was towards undifferentiated NPCs. To identify the main splicing
235 events that explained the observed splicing pattern, we calculated the loadings of the
236 original variables included in the PCA on both PC1 and PC2 (Figure 3b). This analysis
237 revealed numerous genes that are highly relevant for neuronal development.
238 Interestingly, some genes with the highest loadings were associated with
239 neurodevelopmental diseases. For instance, *Shank1* and *Dlgap4* are related to autism
240 spectrum disorder[37,38], whereas *Dlg2* has been linked with schizophrenia[39].
241 To gain insight into the biological processes regulated by the genes that were
242 correlated with each principal component, we performed a gene set enrichment
243 analysis (GSEA) of gene ontology (GO) terms. The loadings of the alternative splicing
244 events on each principal component were used as effect sizes in the GSEA (Figure
245 3c). PC1 was associated with higher-level GO terms such as “regulation of
246 transportation”, “animal organ development”, and “central nervous system
247 development”. This association is plausible given that PC1 represented 55.61% of the
248 variability and separated the samples from early embryonic stage E14.5 to the
249 prepubescent stage P30. During this broad period, manifold biological processes
250 occur, shaping the development of the central nervous system. The higher-level GO
251 terms reflected this complexity as descriptors for the wide-ranging changes captured
252 by PC1. More specifically, transport and localization were significantly enriched for
253 PC1. Interestingly, some splicing events with high PC1 loadings were associated with
254 multiple enriched GO terms. For instance, *Cadps*, a calcium-dependent segregation
255 activator, that was associated with 7 GO terms (Supplementary Data 3), was previously
256 reported to be differentially spliced upon *Rbfox2*-knockout[23]. This gene was also
257 among the top correlated genes of PC1 (Figure 3b, left). Another important gene
258 associated with 6 GO terms was *Ap2a1*. While PTBP2 was previously reported to
259 induce exon skipping in *Ap2a1* (chr7:44,552,885-44,552,951, Supplementary Figure
260 S5a) during brain development[40], *Rbfox2*-OE led to the opposite effect of exon
261 inclusion (FDR < 0.0001, ΔPSI = 0.297) in our data.
262 Moreover, neuron differentiation was among the significant terms associated with PC2,
263 where the *Rbfox2*-OE samples were more similar to an NPC splicing pattern. When
264 analyzing the splicing events that significantly contributed to this GO term, we identified
265 several developmentally relevant genes. For instance, *Clasp2*, a protein involved in
266 microtubule dynamics, is known to play a role in neuronal migration and axonal growth
267 during cortical development[41]. We detected an alternatively spliced exon in *Clasp2*
268 (chr9:113,691,503-113,691,530, Supplementary Figure S5b) that showed a
269 significantly higher inclusion in the *Rbfox2* overexpression group (FDR < 0.0001, ΔPSI
270 = 0.118). Interestingly, we observed a similar increase of the same exon when

analyzing the splicing changes between NPCs and neurons (FDR < 0.01, ΔPSI = 0.118).

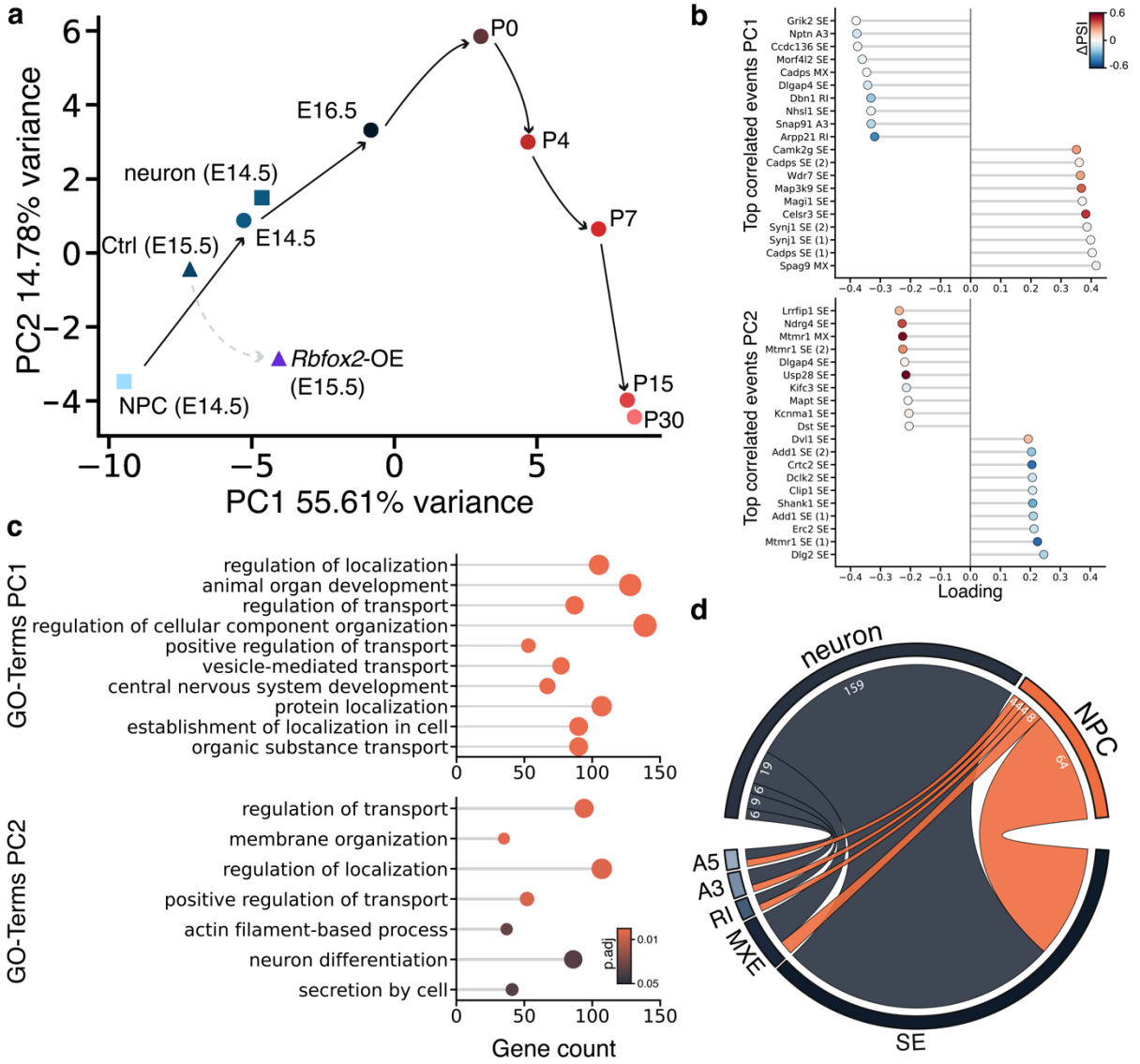

Figure 3 Developmental regulation of alternative splicing by RBFOX2. a) Principal Component Analysis (PCA) of splicing patterns using SplicePCA[42] across embryonic and postnatal brain development. Blue color dots represent embryonic and red dots denote postnatal stages. Shapes indicate the source of the data used. Circles correspond to E14.5 to P30 samples from Weyn-Vanhentenryck et al.[34], squares represent NPC and neuron samples from Liu et al. [43]. Rbfox2 overexpression (OE) samples (triangle shape) noticeably deviate from the expected developmental trajectory. b) Loading analysis for PC1 and PC2, highlighting the top 10 positively and top 10 negatively correlated splicing events for each PC. Color gradient represents the ΔPSI values for Rbfox2-OE compared to control samples c) Gene Set Enrichment Analysis (GSEA) performed on splicing events for PC1 and PC2 using loadings on each component as effect sizes. D) Chord plot showing the association between significant splicing events in Rbfox2-OE vs. control samples compared with splicing events in neurons vs. NPCs obtained using the data from Liu et al. [43].

The observed mixed phenotype upon *Rbfox2*-OE was not only characterized by the deviation from the expected developmental trajectory but also by the type of splicing events. When comparing the significant splicing events upon *Rbfox2*-OE with those of neurons vs. NPCs from the Liu et al. data[43], we found an overlap of 283 significant events. Strikingly, 70% of the events corresponded to a neuron-like splicing and 30% of events represent NPC-like splicing patterns (Figure 3d). Several of the overlapping genes have been reported previously to undergo alternative splicing during important developmental processes associated with NPC proliferation, radial migration of neurons, and neuronal differentiation[8]. Genes with a neuron-like splicing included

Clasp2, *Dctn1*, *Kif2a*, *Mast2*, and *Tpm1*. In contrast, *Add1*, *Clip1*, *Clasp1*, *Dync1i2*, *Gphn*, and *Macf1* were spliced in an NPC-like way (Supplementary Data 4).

RBFOX2 misexpression impairs neuronal differentiation in the embryonic neocortex

After ascertaining the dramatic effect of *Rbfox2* overexpression on the splicing landscape of the developing neocortex, next, we investigated whether this translates into changes in neuronal differentiation and/or migration at the cellular level. Therefore, we electroporated *Rbfox2* constructs into the E13.5 neocortex and analyzed brain sections two days later by immunostaining experiments. We detected significantly more RBFOX2-OE cells in VZ and lIZ. Conversely, we observed significantly fewer RBFOX2-overexpressing cells in the uIZ and the CP (Figure 4a). In line with the observed phenotype of cells detaching from the ventricular surface and subsequently failing to migrate to the cortical plate and accumulating in the lIZ, *Rbfox2-OE* induced alternative splicing of two key constituents of the Reelin pathway which plays an important role during cortical development by guiding neurons to the correct position in the CP[44]. Specifically, an exon of *Lrp8* encoding the murine-specific eighth LDL receptor type A (chr4:107,705,477-107,705,600, Supplementary Figure S5f) was abnormally included (FDR < 0.0001, ΔPSI = 0.275). Expression of this exon was previously linked to neuronal migration[45]. Additionally, the exon (chr19:27,217,244-27,217,370, Supplementary Figure S5g) of *Vldlr* encoding the calcium-binding EGF domain was repressed following *Rbfox2*-OE (FDR < 0.0001, ΔPSI = -0.201). Repression of the EGF domain alters the binding affinity to ligands modulating the sensitivity of the receptor and its interacting ligands[46]. Moreover, RBFOX2 could synergistically act with NOVA2 which is known to induce alternative splicing changes in *Dab1*. DAB1 constitutes a switch within the Reelin pathway that is required for neuronal migration[47,48].

To investigate the impact of *Rbfox2* misexpression on neuronal differentiation, we performed immunostainings with antibodies against the marker genes PAX6 (radial glia cells), TBR2 (basal progenitors), and SATB2 (neurons). This revealed a significant differentiation defect in the *Rbfox2* overexpressing neocortex. In particular, the percentage of $PAX6^+$ radial glial cells and $TBR2^+$ basal progenitors was significantly increased compared to the control group (Figure 4b,c) whereas the percentage of $SATB2^+$ neurons was reduced (Figure 4d). This indicates that a correct and fine-tuned expression of RBFOX2 is essential for proper neuronal differentiation in the embryonic neocortex.

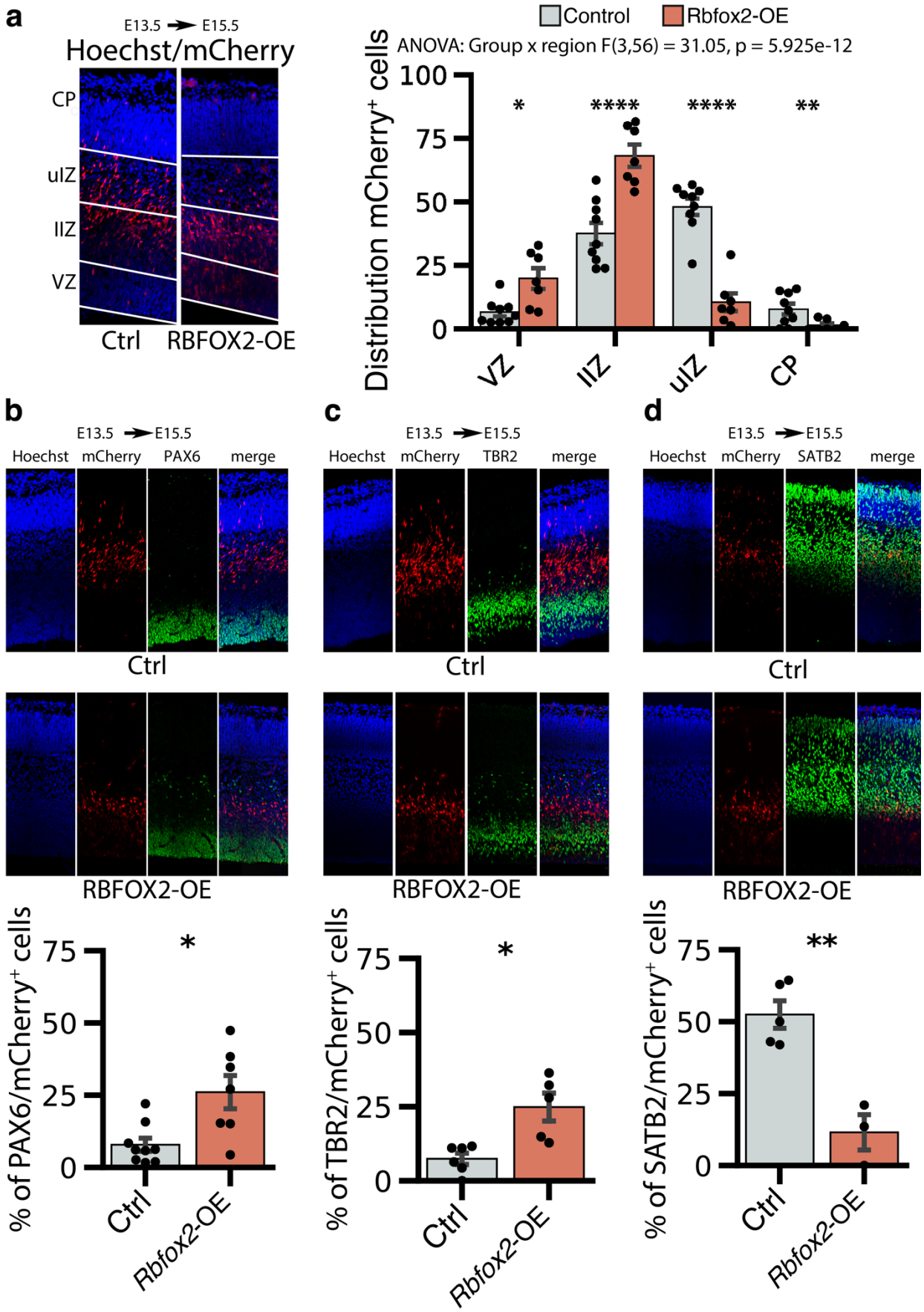

Figure 4 Rbfox2 mis-expression disrupts neuronal differentiation in the neocortex. *Rbfox2 expression constructs were co-electroporated* with *pCAG-mCherry at E13.5. The electroporated brains were analyzed 48 hours later.* a) Distribution of the electroporated mCherry+ cells in the embryonic neocortex. b-d) Cryosections of the electroporated brains were immunostained for markers (green) for radial glia cells (b; PAX6), basal progenitors (c; TBR2) and

neurons (d; SATB2). Bar plots show mean values ± standard error of the mean. * $p<0.05$, ** $p<0.01$, **** $p<0.0001$, two-way ANOVA followed by pairwise comparison of model means in a; * $p<0.05$, ** $p<0.01$, unpaired t-test in b-d.

RBFOX2 canonical and non-canonical motifs are enriched around alternatively spliced exons

Previous studies have shown that RBFOX1, RBFOX2, and RBFOX3 preferably bind to the conserved sequence (U)GCAUG[49,50]. RBFOX's effect is position-dependent – an upstream intronic binding leads to exon repression, while downstream intronic binding enhances exon inclusion (Figure 5b)[51]. Therefore, we expected to find the canonical motif to be enriched at either location according to the type of alternative splicing events. We screened for all possible pentameric motifs in the 150 nt intronic region directly flanking alternatively spliced cassette exons, accounting for their occurrence in three distinct categories: significantly spliced-in (inclusion), significantly skipped (repression), and unregulated exons (background). To mitigate bias from motifs with higher genome-wide occurrence, we adjusted motif counts of significant splicing events by subtracting background counts and subsequently converted these to z-scores (see Methods).

As expected, the canonical RBFOX motif was enriched downstream of included exons and upstream of repressed exons (Figure 5a). The motif GCAUG was associated with the strongest enrichment, both for upstream binding & exon repression (z-score: 6.8) and downstream binding & exon inclusion (z-score: 9.4). Moreover, shifted motifs such as UGCAU and CAUGC were also enriched and had a high correlation with GCAUG ($r > 0.8$; Supplementary Figure S6). Subsequently, we analyzed the position of the canonical GCAUG for exon inclusion and repression events (Figure 5c). We discovered motifs that promote exon skipping, located both within ~100 nt upstream of the alternatively spliced exon and on the exon itself. Exon inclusion was related to GCAUG occurrence within ~150 nt downstream of the exon. These findings are in line with previous reports on the position-dependent splicing activity of RBFOX2[52,53].

However, we found additional motifs known to be bound by other splicing factors. For instance, UGCUU (z-score 4.9, downstream & exon inclusion) is the preferred motif of muscleblind-like splicing regulator 1 (MBNL1). MBNL1 and RBFOX2 have been found to act synergistically in pluripotent stem cell differentiation[54] and mesenchymal-specific splicing[55]. The relative abundance of MBNL1's motif UGCUU around alternatively spliced exons was only weakly correlated with the abundance of the GCAUG motif ($r=0.27$), therefore both motifs were likely not in close proximity to each other (Supplementary Figure S6).

Surprisingly, we also detected highly enriched poly CU-motifs upstream of included exons, although these are not primary binding sites for RBFOX2. The PTB proteins are known to preferentially bind to these polypyrimidine-rich intronic sequences[56] and to initiate exon exclusion upon binding[57]. Interestingly, these PTBP motifs were enriched upstream of significantly included exons in our data.

To differentiate motifs that are merely abundant around RBFOX2-regulated exons, we analyzed publicly available RBP-RNA interaction data (iClip)[52]. Most of the enriched motifs around alternatively spliced exons upon *Rbfox2*-OE were also confirmed to be bound by RBFOX2 in the iClip data (Figure 5d), specifically the known canonical RBFOX motifs showed high positive z-scores for both data sets. Overall, there was a high correlation between the abundance of motifs around alternatively spliced exons and their presence in iClip peaks (Figure 5e).

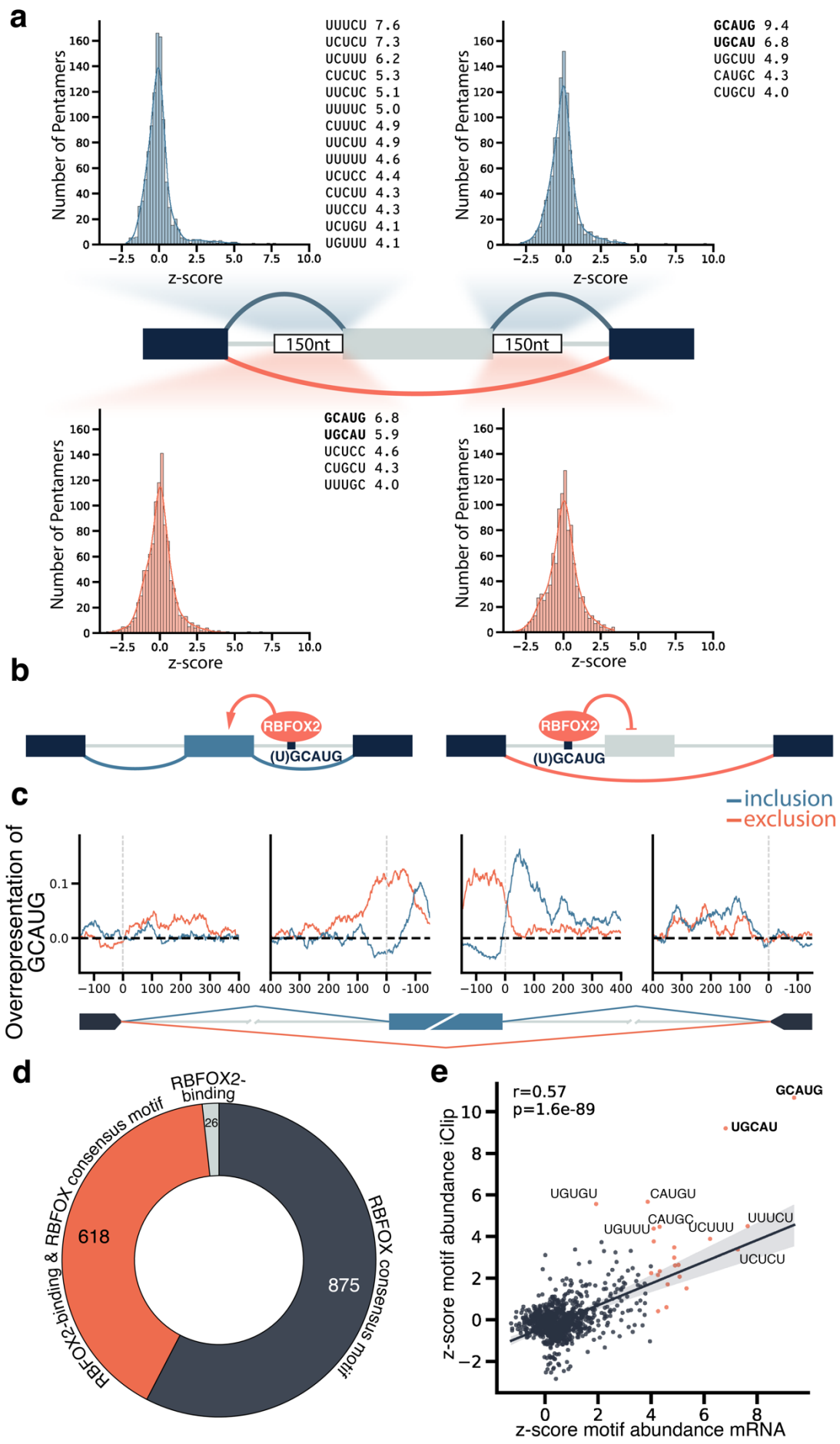
a
Number of Pentamers
z-score
UUUCU 7.6
UCUCU 7.3
UCUUU 6.2
CUCUC 5.3
UUCUC 5.1
UUUUC 5.0
CUUUC 4.9
UUCUU 4.9
UUUUU 4.6
UCUCC 4.4
CUCUU 4.3
UUCCU 4.3
UCUGU 4.1
UGUUU 4.1
GCAUG 9.4
UGCAU 6.8
UGCUU 4.9
CAUGC 4.3
CUGCU 4.0
150nt
150nt
GCAUG 6.8
UGCAU 5.9
UCUCC 4.6
CUGCU 4.3
UUUGC 4.0
b
RBFOX2
(U)GCAUG
RBFOX2
(U)GCAUG
c
inclusion
exclusion
Overrepresentation of GCAUG
d
RBFOX2-binding
26
RBFOX consensus motif
875
RBFOX2-binding & RBFOX consensus motif
618
e
r=0.57
p=1.6e-89
GCAUG
UGCAU
UGUGU
CAUGU
UGUUU
CAUGC
UCUUU
UUUCU
UCUCU
z-score motif abundance iClip
z-score motif abundance mRNA

382

Figure 5 RBFOX2 binding motifs are enriched in the vicinity of alternatively spliced exons. a) Histogram with the frequency of enriched pentameric motifs around alternatively spliced exons in Rbfox2 overexpression (OE) samples versus control. Blue color denotes motifs associated with exon inclusion, while orange represents motifs linked to exon skipping. Known RBFOX2 motifs are indicated with bold font b) Schematic representation of the position-dependent splicing of skipping exons by RBFOX2. c) Relative abundance of the RBFOX2-motif GCAUG in the vicinity of alternatively spliced exons and their flanking exons d) Analysis of alternatively spliced cassette exons reveals that 96% either host an RBFOX motif in the flanking intronic sequence or are bound by RBFOX, as confirmed by iClip data[52]. e) Correlation for the position-dependent prevalence of motifs enriched upstream or downstream of alternatively spliced exons in Rbfox2-OE vs. control comparison and in iClip data[52]. Motifs with high correlation are likely recognized by the same splicing factor.

RBFOX2 and PTBP antagonistically shape the transition from NPCs to neurons

The occurrence of the PTBP motifs upstream of significantly spliced-in exons upon *Rbfox2* overexpression hints at antagonistic splicing activities of RBFOX2 and PTBP (Figure 6a). Previous studies have indicated that PTBPs bind to pyrimidine-rich sequences located approximately up to 100 nt upstream of alternatively spliced exons[9,53]. Accordingly, we observed a prominent UCUCU peak in the ~100 nt intronic sequences upstream of exon inclusion events (Figure 6b). Notably, in experiments involving human brain tissue, cell lines, and the mouse cerebral cortex, the upstream occurrence of the PTBP motif was robustly correlated with exon inclusion events. In contrast, in other tissue types, the upstream enrichment of the PTBP motif was associated with exon-skipping[8,53].

These results raise the question of why a potential upstream PTBP binding leads to exon inclusion rather than the expected exclusion in cells of the nervous system.

We thus hypothesized that simultaneous downstream binding of RBFOX2 might antagonistically overrule the splicing outcome of PTBP and therefore favor exon inclusion. This process could contribute to guiding the transition from immature to mature neuronal splicing. Moreover, PTBP1 and PTBP2 are among the high-confidence protein interaction partners of RBFOX2 (Figure 6c). To investigate whether PTBP and RBFOX2 have antagonistic splicing targets, we first examined all significant cassette exon inclusion events (FDR < 0.01, ΔPSI > 0.1) for the co-occurrence of RBFOX and PTBP motifs. We screened for PTBP-motifs upstream and RBFOX-motifs downstream of alternatively spliced exons and for direct RNA-protein binding sites by reanalyzing iClip data from Vuong et al. for PTBP1[40] and PTBP2[40] and Jangi et al. for RBFOX2[52]. Roughly 45% of the significant inclusion events (320) had the combination of RBFOX-motif downstream with a PTBP-motif upstream, the majority of these were also highly conserved (Supplementary Figure S7). The cassette exons that were significantly included rarely contained only an RBFOX motif (3) or its binding site (0). The majority of included exons, making up 77.48% (547) of the alternatively spliced exons, harbored either a downstream RBFOX-motif and/or an RBFOX-binding site and simultaneously an upstream PTBP-motif or a PTBP-binding site (Figure 6d). While previous studies have indeed highlighted an interaction between RBFOX and PTBP1 specifically[8,58–61], the co-regulation of these RBPs may be less relevant in the context of neurodevelopment, as PTBP1 is primarily expressed in non-neuronal cells[17]. Thus, we only focused on PTBP2 in our further analyses.

To corroborate the RBFOX2/PTBP2 antagonistic splicing regulation of cassette exons, we re-analyzed wildtype and *Ptbp2*-KO data of P1 mouse neocortices[40]. We detected 707 significantly alternatively spliced exons in *Ptbp2*-KO (429 included, 187 excluded), with 128 events shared with *Rbfox2*-OE. This represented a 5.241-fold enrichment compared to the expected overlap ($p < 0.0001$, Supplementary Figure 8a). Given the

434 proposed antagonistic relationship between both RBPs, we expected *Ptbp2* knockout
435 to induce similar splicing changes as *Rbfox2* overexpression. Indeed, the majority of
436 shared target exons were spliced in the same direction (85.2%, Supplementary Figure
437 8c). Furthermore, we observed a moderate positive correlation between exon inclusion
438 levels in *Ptbp2*-KO and *Rbfox2*-OE samples ($R = 0.2993$, $p < 0.001$, Supplementary
439 Figure 8b). To further investigate the neurodevelopmental relevance of antagonistic
440 splicing, we analyzed the splicing pattern in our data of 230 PTBP2-repressed exons
441 that were reported to be relevant specifically in the context of neocortical
442 development[40]. *Rbfox2*-OE induced alternative splicing in 67 of these PTBP2 targets.
443 Importantly, the majority of the 67 significant events showed exon inclusion (55) and
444 not exon repression in the *Rbfox2*-OE group (Figure 6e, Supplementary Data 5).
445 Among the antagonistically spliced genes was *Ncam1,* encoding for a cell adhesion
446 protein*,* that showed an abnormal early exon inclusion (FDR < 0.0001, ΔPSI = 0.148)
447 in the *Rbfox2*-OE condition which led to an increased presence of the exon18
448 (chr9:49,418,152-49,418,953, Supplementary Figure S5c) producing the NCAM-180
449 isoform. Interestingly, the production of alternative isoforms of NCAM occurs during
450 cortical development between E16.5 and P0. In contrast, NCAM140 and NCAM180
451 are the predominant isoforms for neurons, unlike NPCs that express NCAM120 and
452 NCAM140[62].
453 Another PTBP2-excluded[40] and RBFOX2-included cassette exon event was identified
454 in *Kif21b* (chr1:136,101,209-136,101,389, Supplementary Figure S5d). KIF21B is an
455 important regulator of microtubule dynamics. The overexpression of *Rbfox2* induced a
456 highly significant inclusion event (FDR < 0.0001, ΔPSI = 0.305).

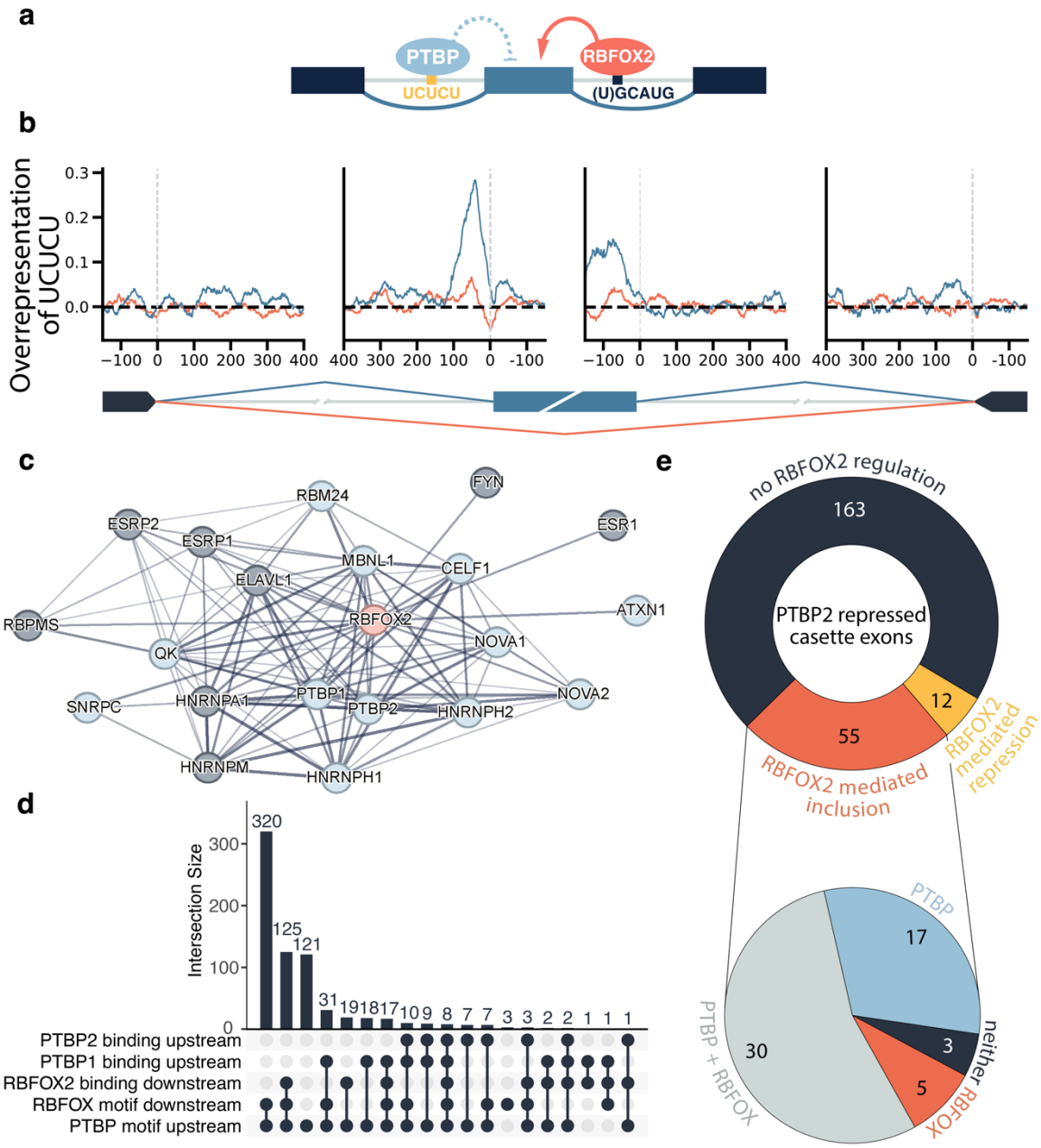

Figure 6 RBFOX and PTBP regulate common targets a) Schematic representation of antagonistic splicing regulation between RBFOX2 and PTBP b) Relative abundance of the PTBP motif UCUCU in the vicinity of alternatively spliced exons in Rbfox2-OE vs. control and their flanking exons. Blue lines indicate exon inclusion and red lines correspond to exon skipping events c) StringDB protein-protein interaction network showing RBFOX2 (orange) and its interaction partners. High-confidence partners are highlighted in light blue d) UpSet plot showing the overlap of the presence of RBFOX or PTBP motifs in the flanking intronic sequences of alternatively spliced cassette exons (400 nt) as well as direct RBFOX2 and PTBP2 binding interactions as indicated by the presence of peaks obtained from iClip data[40,52] e) Analysis of developmentally regulated cassette exons suppressed by PTBP2 and the overlap with significantly alternatively spliced exons upon Rbfox2-OE. The donut-shaped circle represents 230 neurodevelopmentally relevant PTBP2-repressed cassette exon events[40]. Colors indicate regulation of these exons upon Rbfox2-OE, blue: unregulated, orange: inclusion, yellow: repression. The lower circle summarizes the presence of conserved binding motifs for RBFOX2 and/or PTBP2 for the exons that are regulated in opposite direction by PTBP2 (repression) and RBFOX2 (inclusion).

Furthermore, exonN (chrX:73,284,421-73,284,478) of the *Flna* transcript was significantly included (FDR < 0.05, ΔPSI = 0.213) upon *Rbfox2*-OE (Supplementary Figure S5e). ExonN was specifically repressed in NPCs and included in neurons (FDR < 0.0001, ΔPSI = 0.4) and the exon inclusion was strongly elevated from E14.5 to E16.5 (FDR < 0.0001, ΔPSI = 0.4205). The iClip[40,52] data also confirmed protein

476 binding for RBFOX2, PTBP1, and PTBP2 in flanking sequences of exonN. *Flna* is an
477 important regulator of neuronal migration[63] and its splicing by PTBP1 in NPCs is
478 associated with shaping the NPC-to-neuron transition during cortical development[8,40].
479 Taken together, our data strongly suggest that RBFOX2 and PTBP2 have antagonistic
480 roles in controlling alternative splicing, specifically affecting transcripts implicated in
481 neuronal differentiation during cortical development. We identified that a significant
482 portion of alternatively spliced cassette exons are excluded upon PTBP2- but included
483 upon RBFOX2-binding in this developmental context.
484

485 miR-92a-3p regulates the expression of *Rbfox2*

486 As we ascertained, NPCs exhibit substantially different splicing patterns compared to
487 neurons (Supplementary Figure S2)[8,43]. Since RBFOX and PTB proteins seemingly
488 regulated antagonistically an overlapping set of developmentally relevant splice
489 targets, we hypothesized that a cell-type, spatially divergent, and time-specific
490 expression of these splice factors would be necessary for normal cortical development.
491 Indeed, *Ptbp1* and *Ptbp2* transcription peaked at E14.5, but contrary to *Ptbp2,* the
492 *Ptbp1* mRNA abundance decreased in the following developmental stages (Figure 7a,
493 right box). Moreover, *Ptbp1* expression is decreased significantly during the transition
494 from NPCs to neurons (Figure 7a, left box) in accordance with previous reports[40,56,64].
495 *Ptbp1* repression is mediated via miR-124-3p, which is a highly specific neuronal
496 miRNA (Figure 7c)[17,65]. Furthermore, miR-124-3p becomes significantly up-regulated
497 in the transition between E14 and E17 of cortical development (Figure 7c)[65].
498 In contrast to *Ptbp1* and *Ptbp2*, *Rbfox2* expression was nearly absent in NPCs and
499 increased significantly in neurons (Figure 1a-b, Figure 7a). In a previous study, we
500 identified 36 miRNAs that were expressed in the embryonic cerebral cortex and
501 predicted to target the 3' untranslated region (3' UTR) of *Rbfox2.* By further inspecting
502 these miRNAs, we observed that most of them were upregulated at E14 followed by a
503 significant reduction of expression levels at the subsequent developmental stages E17
504 and P0 (Supplementary Figure S9)[65]. This prompted us to hypothesize that miRNAs
505 might mediate the low expression levels of *Rbfox2* in NPCs. Specifically, miR-92a-3p
506 was identified as a hub microRNA at E14 during cortical development[65] and it has a
507 predicted binding site in the 3' UTR of *Rbfox2.* Furthermore, the expression of miR-
508 92a-3p was higher in NPCs compared to neurons and decreased gradually from E14
509 to P0 (Figure 7c). Together this data suggests that miRNA-92a-3p might contribute to
510 silencing *Rbfox2* in NPCs at early developmental stages.
511 To follow up on this hypothesis, we performed a luciferase assay using a fragment of
512 the 3' UTR of *Rbfox2* which contained the miR-92a-3p binding site downstream of the
513 *Renilla* luciferase gene. Co-transfection of this reporter plasmid into HEK293 cells
514 together with a miR-92a-3p mimic or a control revealed a reduced luciferase activity of
515 more than two-fold in cells transfected with miR-92a-3p compared to the control. This
516 finding confirmed the gene silencing effect of miR-92a-3p on *Rbfox2* ($p < 0.01$, Figure
517 7d). To investigate the mir-92a-3p-mediated suppression of *Rbfox2 in vivo,* we
518 electroplated mouse embryos at E14.5 with a miR-92a-3p-silencing construct.
519 Expression of miR-92a-3p was reduced more than 10-fold compared to control
520 samples ($p < 0.0001$, Figure 7e). Following miR-92a-3p reduction, we observed a
521 significantly increased *Rbfox2* expression at E16.5 in the miR-92a knock-down
522 samples compared to the control ($p < 0.01$, fold change = 1.571; Figure 7e). To further
523 corroborate these results, we overexpressed miR-92a-3p in an N2A cell culture. This
524 resulted in a significant increase of miR-92a-3p abundance, as measured by RT-qPCR

(p < 0.05, fold change = 2.442; Figure 7f). Importantly, both the mRNA expression (p < 0.05, fold change = 0.748 relative to control; Figure 7f) and the protein levels of RBFOX2 (p < 0.05, fold change = 0.707 relative to control; Figure 7g,h) were reduced significantly upon miR-92a-3p-overexpression.

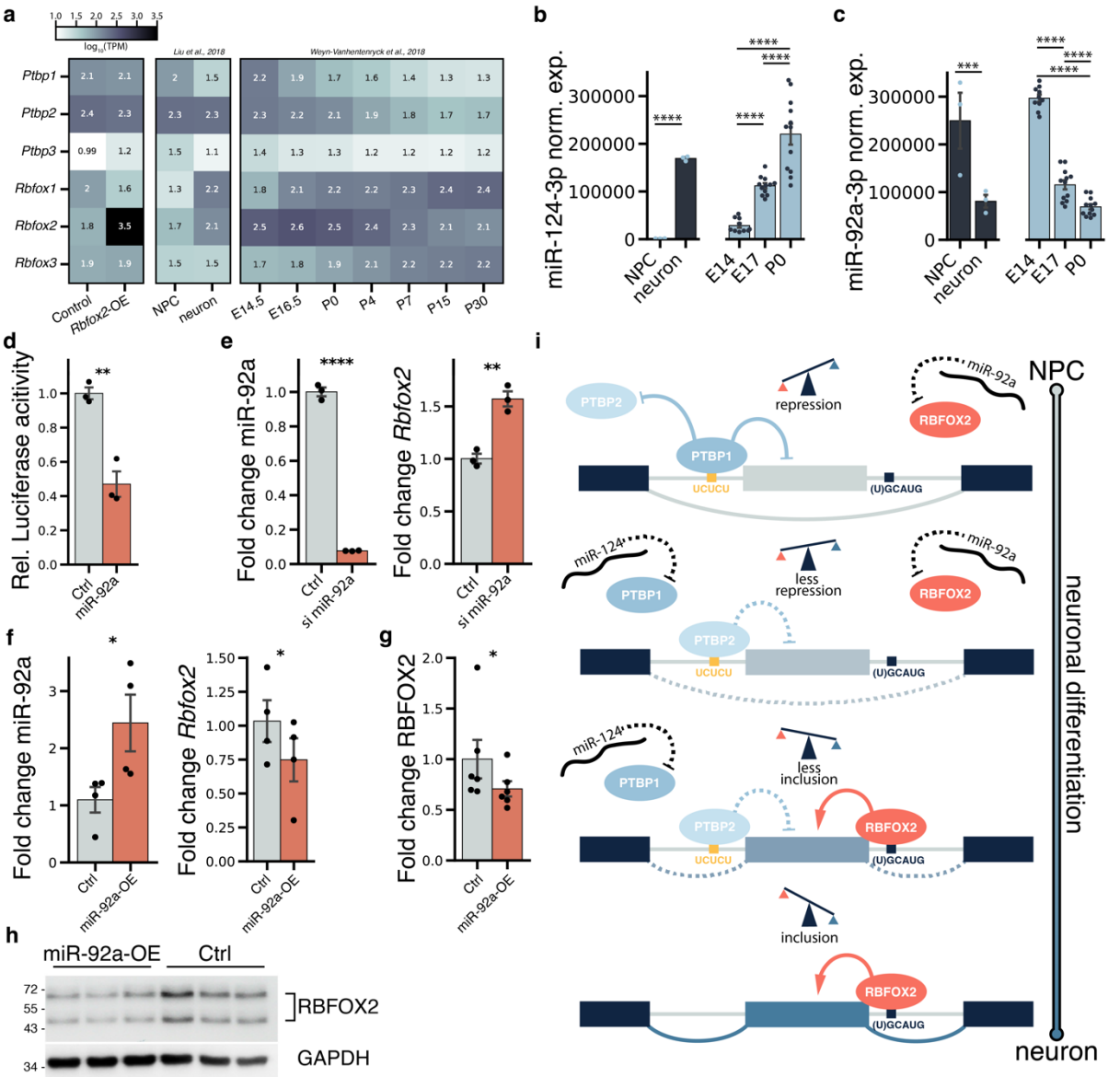

*Figure 7 a) Heatmap showing the gene expression of the RBFOX and PTBP protein families in our study, as well as in NPCs and neurons from Liu et al. [43] and E14.5 to P30 cortical samples obtained from Weyn-Vanhentenryck et al.[34]. Values correspond to log10-transformed transcripts per million (TPM). b) Expression of mir-124-3p known to repress Ptbp1 c) Expression of mir-92a-3p predicted to target Rbfox2. Data on miRNA expression shown in b and c were obtained from Todorov et al.[65] d) Luciferase activity in lysates of HEK293 cells transfected with plasmids containing 3' UTR fragments of Rbfox2 and miR-92a. Fold change of luciferase activity was obtained by calculating the ratio of Renilla luciferase and firefly luciferase activity and then normalizing to the mean of the control. e) In vivo knock-down of miR-92a resulted in a more than 10-fold reduction in miR-92a-3p abundance (left side), and subsequently, Rbfox2 was 1.5-fold enriched (right side). f) Overexpression of miR-92a-3p in N2A cells led to >2-fold enrichment of miR-92a-3p (left side) and subsequently to a decreased abundance of Rbfox2 (right side), as measured by RT-qPCR. h) Overexpression of mir-92a-3p in N2A cells reduced the RBFOX2 protein level significantly. g) Representative image of the western blot for miR-92a overexpression in N2A cells. h) Schematic representation of the proposed splicing mechanism for the transition of immature NPC to mature neurons. Data are shown as mean ± standard error of the mean. *p<0.05, ** p<0.01, *** p<0.001, ****p<0.0001, Wald z-test from DESeq2 in b,c; paired t-test or paired Wilcoxon test in d-g.*

Discussion

RBFOX2 is a crucial component of the complex regulatory network that orchestrates cerebral cortical development. We revealed that misexpression leads to a global disruption of the alternative splicing landscape with a significant overrepresentation of high-confidence NDD risk genes. Consequently, aberrant RBFOX2 splicing activities could produce target gene isoforms that lead to impaired brain development and disorders of the central nervous system in humans[66,67]. For instance, a mutation in *RBFOX2* has been detected previously in a patient with hypoplastic left heart syndrome and NDD[21]. Surprisingly, however, limited research has been conducted on the clinical significance of RBFOX2 as most studies focus on RBFOX1. Mutations in *Rbfox1* have been consistently linked with autism spectrum disorder[68–71] and susceptibility to epilepsy[72–74]. Interestingly, *Rbfox1* knock-out resulted in higher seizure susceptibility[75], whereas overexpression was also linked with epilepsy and cortex malformation[76]. Furthermore, reduced cytoplasmic RBFOX1 levels in the prefrontal cortex of individuals with schizophrenia[24] decrease the stability of *Vamp1*, a schizophrenia-associated gene, in PV^+ interneurons[25]. This reduction impairs inhibitory drive from PV^+ interneurons, contributing to schizophrenia pathogenesis[77].

Though RBFOX1 and RBFOX2 have largely overlapping alternative splicing targets[49], the divergent expression patterns we observed here and in previous research indicate that both proteins have common but also distinct functions[23,75,78,79]. To disentangle the specific role of RBFOX2 in the developing brain, we employed an overexpression model instead of a knock-down strategy, as the members of the RBFOX family can compensate for the absence of one of their paralogues[23]. Interestingly, early *Rbfox2*-OE caused a premature detachment and migration of neural cells to the IIZ but not further (Figure 4a). This was accompanied by significant splicing events in key components of the Reelin pathway[44,45] , which plays a crucial role in the migration and localization of cortical neurons and Purkinje cells in the cerebellum. Gehman and colleagues previously showed that the Reelin-binding *Lrp8* gene was alternatively spliced upon *Rbfox2* knock-out. Consequently, Purkinje cells failed to detach and therefore remained near their origin in the VZ[23]. Together with our results, this indicates an important role of RBFOX2 in the initiation and control of cell migration in different parts of the developing nervous system.

Apart from the altered migration, we also observed impaired neuronal differentiation of *Rbfox2*-overexpressing cells (Figure 4b-d). RBFOX2 was specifically upregulated in the transition from NPCs to newly differentiated neurons (Figure 1e), highlighting its role in neural differentiation. Accordingly, we detected a strong alternative splicing pattern in *Numb* which is a key player in asymmetrical neural stem cell division, determining the cell fate of progenitor cells and neurons[80]. Different isoforms of *Numb* can either promote neuronal differentiation or enhance cell proliferation[81], giving a possible explanation for the observed phenotype of decreased neuronal differentiation in our study.

Interestingly, *Rbfox2* expression negatively correlates with expression patterns of the PTBP family. In particular, PTBP1 is a key regulator of non-neuronal splicing in progenitor cells and its repression is required to induce the transition to neurons[17]. In contrast, PTBP2, which is reported to be a weaker repressor of alternatively spliced exons than PTBP1[57,82], is down-regulated by PTBP1 via poison exon inclusion leading to nonsense-mediated decay[17,52,64,83]. Remarkably, our data provided compelling evidence for an antagonistic splicing relationship between RBFOX2 and PTBP2.

595 Specifically, RBFOX2 and PTBP2 shared a set of targets that undergo alternative
596 splicing during cerebral cortical development (Figure 6d, e). Although PTBP2 typically
597 promotes the exclusion of these antagonistically spliced exons, RBFOX2 induced the
598 opposite effect of exon inclusion. Therefore, the premature overexpression in our
599 experimental set-up likely led to RBFOX2 overruling the splicing program of PTBP2
600 which could explain the aberrant cellular phenotype and altered splicing landscape we
601 observed. Indeed, several targets that are spliced antagonistically between RBFOX2
602 and PTBP2 play crucial roles, for example, in regulating neuronal differentiation
603 (*Flna*)[8], neurite outgrowth (*Ncam1*), and microtubule dynamics (*Kif21b*). Furthermore,
604 PTBP-recognized motifs are reportedly enriched upstream of alternatively spliced
605 exons that show high inclusion levels in the brain, heart, and skeletal muscles[53]. These
606 tissues are known expression sites of RBFOX2[84] with a concurrent low expression of
607 PTBP1[53]. Therefore, our results and existing reports highlight a complex antagonistic
608 interplay between these proteins in regulating neuronal differentiation[4,8]. Supporting
609 the concept of such dose-sensitive antagonistic interactions among RNA-binding
610 proteins, Ellis and colleagues recently reported that even a modest increase in RBFOX
611 expression levels was sufficient to alter splicing events dependent on another RBP,
612 MBNL1[85]. Furthermore, RBFOX-concentration-dependent splicing regulation has been
613 described in relation to binding to secondary motifs. Accordingly, high RBFOX2 protein
614 levels during neuronal differentiation can mediate exon inclusion through binding to
615 low-affinity motifs[86]. These findings illustrate how nuanced temporal and spatial RBP
616 expression levels enable cell- and developmental-stage specific gene regulation during
617 brain development.
618 Indeed, several post-transcriptional regulatory mechanisms controlling RBFOX levels
619 have been reported already. For instance, snoRNAs can act as sequestering sites for
620 excess RBFOX2 proteins[78]. Furthermore, RBFOX3 can splice poison exons into
621 *Rbfox2* leading to NMD[87]. Another potential layer of regulation is a putative *Rbfox1*-
622 and *Rbfox2*-specific feedback loop. Accordingly, we observed significantly reduced
623 levels of *Rbfox1* following the overexpression of *Rbfox2* (Figure 2g). Similarly, a knock-
624 out of *Rbfox1* was previously reported to lead to an increased level of RBFOX2[75] and
625 vice versa[23]. Furthermore, both RBFOX1 and RBFOX2 contain RBFOX binding sites
626 near a highly conserved 93-nucleotide exon encoding the second half of the RRM.
627 RBFOX binding leads to exon skipping, thereby resulting in a *Rbfox*ΔRRM isoform with
628 significantly reduced RNA binding affinity[88]. In line with this, the *Rbfox2* overexpression
629 in early-stage cortical cells in our study did not result in a complete splicing switch with
630 all regulated exons being either fully spliced in or spliced out.
631 miRNA binding to 3' UTRs represents another key post-transcriptional regulatory
632 mechanism for controlling gene expression and protein levels. In a study investigating
633 the expression patterns of miRNAs in the embryonic cerebral cortex, we recently
634 highlighted targeting of RNA binding proteins as one of the major processes through
635 which miRNAs impact brain development[65]. Similarly to the reported silencing of *Ptbp1*
636 in neurons via miR-124-3p[17], here we showed for the first time that the NPC hub
637 miRNA 92a-3p suppresses the expression of *Rbfox2* (Figure 7f-h). Conversely,
638 silencing miR-92a-3p in the embryonic neocortex led to a significant *Rbfox2*
639 upregulation (Figure 7e, i). In accordance with our results, miR-92a-3p was previously
640 reported to be enriched in intermediate progenitor cells in humans[89,90] and,
641 interestingly, differentially expressed in neurodevelopmental and mental disorders. For
642 instance, levels were elevated in blood[91] and serum[92] of patients with schizophrenia.
643 In contrast, miR-92a-3p was reported to be downregulated in individuals with

644 autism[93,94]. Given the overlapping splicing targets between RBFOX2 and its paralogue
645 RBFOX1, whose mutations have been consistently implicated in such disorders,
646 disruption of the miR-92a-3p/RBFOX2 axis represents an intriguing mechanism for the
647 emergence of diseases of the central nervous system as well as a potential therapeutic
648 target. In particular, future research should focus on elucidating the link between
649 altered miR-92a-3p expression levels and aberrant splicing activities that contribute to
650 disease pathogenesis.
651 Collectively, our results underscore the crucial role of RBFOX2 in the developing
652 cerebral cortex and shed light on the complex interplay with the PTBP family. In our
653 proposed model (Figure 7b), a miRNA-mediated gradual shift from high PTBP levels
654 to a subsequent up-regulation of RBFOX2 shapes neuronal differentiation through a
655 progressive splicing switch from exon exclusion to exon inclusion in commonly
656 regulated targets.
657

658 **Methods**

659 Animals
660 Hes5::GFP mice have been described previously[95]**.** For *in utero* electroporation, timed
661 mated c57BL6/JRj female mice were purchased on gestation day 12 from Janvier
662 (Janvier Labs, Le Genest-Saint-Isle, France), a certified international breeder. Mice
663 were housed in type II long filter top cages (Tecniplast, Buguggiate, Italy) and kept in
664 a 12 h light/dark cycle in a temperature and humidity-controlled animal room (22 ± 2°C,
665 55 ± 5%). Water and food (ssniff M-Z Extrudat, ssniff, Soest, Germany) were supplied
666 *ad libitum*. Mice were treated according to the protocols approved by the local
667 authorities (Landesuntersuchungsamt Rheinland-Pfalz, license number 23 177-07/G
668 13-1-089).
669

670 Constructs
671 HA-tagged full-length *Rbfox2* was cloned into the XhoI and BglII sites of the pCAGGS-
672 mCherry vector using the following primer combinations: *Rbfox2* 1A full-length forward
673 5′-actgctcgaggccaccatgtacccatacgatgttccagattacgctgcggaaggcggccaggcg-3′, with
674 *Rbfox2* reverse 5′-actgagatcttcacgtcacttcagtagg-3′. The miR-92a pre-miRNA
675 including approximately 150 bp of flanking genomic sequence was cloned into the
676 BamHI and EcoRI sites of the pcDNA3.1+ vector using the following primer
677 combinations: miR-92 forward 5′-agtcggatcctttagcgttggaaagtggcc-3′ with miR-92a
678 reverse 5′-agtcgaattctaagttgaggtgtgggtggg-3′. A fragment of the *Rbfox2* 3'UTR
679 containing the miR-92a binding site was cloned into the XbaI site of the pGL3P vector
680 using the following 5'-end phosphorylated oligonucleotides: Sense [Phos] 5′-
681 CTAGACCCCAGTTCATGAGGCCTGGCTATTGCAATATTTACTAGTAGAGGACTC
682 TATAGCT-3′, Antisense [Phos] 5′-CTAGAGCTATAGAGTCCTCTACTAGTAAAT
683 ATTGCAATAGCCAGGCCTCATGAACTGGGGT-3′. Sense and Antisense oligos
684 were annealed in annealing buffer (10mM Tris-HCL; pH 7.5; 0.1 M NaCl; 1 mM EDTA)
685 and cloned into the XbaI site of the pGL3P vector.
686

687 Cell Culture, transfections, and luciferase assays
688 N2A and HEK293 cells were cultured in Dulbecco´s Modified Eagle Medium (DMEM)
689 with 10% fetal bovine serum as well as 1% Penicillin/Streptomycin. For Luciferase
690 assays, HEK293 cells were seeded on 12-well plates at a density of 90,000 cells per
691 well. Twenty-four hours later, the cells were transfected with 400 ng of the constructs

692 cloned into the pGL3P vector, 600 ng miRNA construct and 10 ng pRL-TK vector using
693 the calcium phosphate method. After 48 hours, cells were lysed, and luciferase activity
694 was measured with a CentroXS LB 960 luminometer (Berthold Technologies). N2A
695 cells were transfected with Transfectin reagent (Biorad). The day before the
696 experiment. For transfection, N2A cells were seeded at a density of 250,000 cells per
697 well on 6-well plates. Twenty-four hours later, the cells were transfected with 4000 ng
698 miRNA construct per well. The cells were lysed and processed for RT-qPCR and
699 Westernblot analysis 48 hours after transfection.
700

701 RT-qPCR and Western blot

702 Small RNAs were isolated using the miRNeasy Kit (Qiagen), and total RNA was
703 isolated using the High Pure RNA isolation kit (Roche). TaqMan MicroRNA Assays
704 (Applied Biosystems) were used for miRNA RT-qPCR experiments. The miRNA
705 quantities are relative to U6 snRNA. Total RNA was reverse transcribed using the
706 RevertAid First Strand cDNA Synthesis Kit (Fermentas, Sankt Leon Rot, Germany).
707 For qPCR, SYBR Green Mix was used (TB Green Premix Ex Taq II (RR82WR,
708 Takara)).
709 For Western blot analysis, the cells were lysed, and the proteins were resolved by
710 electrophoresis on SDS acrylamide gels. After transferring the proteins to PVDF
711 membranes, Western blot analyses were performed with antibodies specific for
712 RBFOX2 (rabbit-Anti Rbm9; Bethyl Laboratories) and GAPDH (mouse-Anti GAPDH
713 ab8245, Abcam). Quantification of the bands was performed with ImageJ and
714 normalized to GAPDH band intensity.
715

716 *In utero* Electroporation

717 For *in utero* electroporation, embryonic day E13.5 pregnant female mice were deeply
718 anesthetized with isoflurane, and the uterine horns were exposed. For overexpression,
719 control or *Rbfox2* expression vectors (4 μg/μl) were injected with either pCAG-mCherry
720 or pCAG-eGFP (0.5 μg/μl) into the lateral ventricle of each embryo. For electroporation
721 5 pulses of 40 V for a pulse length of 50 ms at 950-ms intervals were applied
722 (Nepagene, Japan). Subsequently, the uterine horns were returned to the abdominal
723 cavity. After 48 h, the mice were sacrificed by cervical dislocation. The embryos were
724 collected and sacrificed by decapitation. For immunostaining experiments, the brains
725 were isolated, fixed in 4% paraformaldehyde, cryoprotected in 15% and 30% Sucrose
726 solutions, embedded in Cryomatrix (Thermo Scientific), and cryosectioned into 20 μm-
727 thick brain slices.
728 For RNA-sequencing, the brain's GFP^+ area was dissected and digested with trypsin.
729 After stopping the digestion by adding 20% FBS in DMEM and washing with PBS, cells
730 were resuspended in PBS and passed through a 100 μm filter to achieve a single-cell
731 suspension. GFP^+ cells were then collected by fluorescent activated cell sorting
732 (FACS).
733

734 Immunostaining and Imaging

735 For immunostaining, brain cryosections were fixed in 4% paraformaldehyde (PFA) at
736 room temperature (RT) for 10 minutes. After two washes with PBS, antigen retrieval
737 was performed by incubating the slides in 10 mM sodium citrate with 0.5% Tween-20,
738 pH 6, at 80°C for 20 minutes. Subsequently, the sections were blocked in PBS with

739 0.2% Tx-100 containing 2% sheep serum. The sections were then incubated with
740 primary antibody (rabbit anti-RBM9 (Bethyl), mouse anti-RBFOX1 (MABE985,
741 Merck/Millipore, Burlington, MA, USA), rabbit anti-beta III Tubulin (ab18207, Abcam),
742 rabbit Anti-PAX6 (901301, Biolegends), chicken Anti TBR2 (ab34735, Millipore), rabbit
743 Anti-SATB2 (ab34735, Abcam)) in blocking solution overnight at 4°C. The sections
744 were washed three times in PBS 0.2% Tx-100 and incubated in blocking solution
745 containing Alexa-488- or Alexa-594-conjugated secondary antibody (Invitrogen) for 3
746 hours at RT. After three washes in PBS, the sections were embedded in Fluoromount-
747 G with DAPI (00-4959-52, Invitrogen).
748 The sections were viewed using a laser-scanning confocal microscope (LSM710), and
749 images were acquired with the zen software (Zeiss, Oberkochen, Germany). The
750 images were analyzed, and the cells were counted using ImageJ software[96].
751

752 RNA-sequencing

753 NGS library prep was performed with Clontech SMARTer Ultra Low Input RNA Kit for
754 cDNA generation, followed by NuGEN Ovation Ultralow v2 System for library
755 preparation. Libraries were profiled in a DNA 1000 chip on a 2100 Bioanalyzer (Agilent
756 Technologies) and quantified using the Qubit dsDNA HS Assay Kit, in a Qubit 4.0
757 Fluorometer (Invitrogen by Thermo Fisher Scientific). All six samples were pooled in
758 equimolar ratio and sequenced on an Illumina NextSeq 500/550 device.
759

760 RNA-sequencing analysis

761 The paired-end reads were trimmed using BBDuk (version 39.01)[97]. The trimmed
762 reads were mapped to the Gencode reference genome of Mus musculus mm39
763 (released 19.10.2022) using STAR (version 2.7.10b)[98] and the count per gene and
764 sample was determined using FeatureCounts provided by SubRead (version 2.0.6)[99].
765 We used DESeq2 (version 1.40.1)[100] in R (version 4.3.0)[101] to analyze differentially
766 expressed genes with default settings. Since *Rbfox2* was heavily overexpressed, it
767 was removed from the volcano plot for improved visualization. Genes with an adjusted
768 p-value (Benjamini-Hochberg method) < 0.05 were considered to be differentially
769 expressed.
770 rMATS (version 4.1.2)[102] with default settings was used to detect alternatively spliced
771 genes between the *Rbfox2*-OE and control samples. We did not include novel splice
772 events in our analysis. A splicing event with a false discovery rate (FDR) adjusted p-
773 value < 0.01 and an inclusion level difference $|\Delta PSI| > 0.1$ was considered significant.
774 Data processing was done with numpy (version 1.23.5)[103] and pandas (version
775 2.0.1)[104] in Python (version 3.10.12)[105].
776 Plots were generated if not specified otherwise with Matplotlib (version 3.7.1)[106] and
777 seaborn (version 0.12.2)[107].
778 The overlap between significantly alternatively spliced genes and significantly
779 differentially expressed genes was visualized in an UpSet plot (version 0.9.0)[108] using
780 Python (version 3.10.12)[105]. Sashimiplots were created using rmats2sashimiplot within
781 a Docker container using the image xinglab/rmats2sashimiplot. Due to its MISO
782 backend, PSI values may differ from rMATS results.
783

784 Analysis of publicly available transcriptomic data sets

785 We re-analyzed two publicly available data sets to further characterize the alternative
786 splicing landscape during cortical development. The study by Weyn-Vanhentenryck et

al. contains RNA-sequencing of the mouse cortex from nine-time points (E14.5, E16.5, P0, P4, P30, 4 months, and 21 months). Sequencing files were downloaded from the NCBI Short Read Archive, accession number SRP055008. The study by Liu et al. contains RNA-sequencing from NPCs and neurons purified from mouse cortices at E15.5, sequencing files were obtained from the Gene Expression Omnibus, accession number GSE96950. Furthermore, we re-analyzed transcriptomic data from *Ptbp2* knockout mouse cortices at P1, obtained from the Gene Expression Omnibus (accession number GSE84803)[40], and triple knockout (*Rbfox*1/2/3) mouse embryonic stem cells, retrieved from the Short Read Archive (accession number SRP128054)[32]. The sequencing data were processed according to the protocol specified under the section "RNA-sequencing analysis". The developmental data from Weyn-Vanhentenryck et al. did not allow a pairwise statistical test with rMATS, therefore we conducted a pairwise Fisher's exact test in scipy (version 1.10.1)[109] for consecutive time points and corrected p-values for multiple comparisons by using Benjamini Hochberg's procedure with scipy (version 1.10.1)[109]. An event was considered significantly developmentally alternatively spliced when two successive time points had an adjusted p-value < 0.01 and $|\Delta PSI| > 0.1$.
We used a Monte Carlo simulation to statistically assess the overlap of alternative splicing events (cassette exons) between *Rbfox2*-OE and either t*Rbfox*-KO[32] or *Ptbp2*-KO[40] conditions (see Monte Carlo simulation for details).

Analysis of publicly available iClip data sets

To validate which significant splicing events could be attributable to direct RBFOX2 binding, we re-analyzed publicly available iClip data for RBFOX2 expressed in V6.5 mESCs. The data was downloaded from NCBI Gene Expression Omnibus, accession number GSE54794[52]. This dataset was supplemented by iClip data for PTBP1 and PTBP2, downloaded from the NCBI short read archive, accession number SRP080878[40].
The iClip data was analyzed in several steps. First, we extracted the unique molecular identifiers from the reads using UMI tools (version 1.1.4)[110] and trimmed the adapters with BBDuk (version 39.01)[97]. The trimmed reads were aligned to the reference genome mm39 from Gencode (released 19.10.2022) using STAR (version 2.7.10b)[98]. Following the alignment, we removed PCR duplicates by leveraging the unique molecular identifiers with UMI tools. Crosslinking sites were identified as peaks using Clipper[111], which was run within a Docker container based on the image brianyee/clipper:61d5456.

Inferring the alternative splicing trajectory during cortical development

We used the SplicePCA tool[42] integrating our data set with the developmental data of Weyn-Vanhentenryck et al.[4] and Liu et al.[29] to analyze the effect of *Rbfox2*-overexpression on the alternative splicing pattern compared to normal cortical development. We selected events that did not have missing data for any sample and were significantly alternatively spliced in our data and the publicly available data. To investigate how splicing events are correlated with the principal components, we then computed the loading matrix A

$$qA = V\sqrt{L}$$

where V is the matrix of eigenvectors, L is a diagonal matrix with the corresponding eigenvalues and loadings correspond to correlations between the principal components and the original variables[112].

836 For each principal component, we then performed a gene set enrichment analysis
837 (GSEA) using the clusterProfiler package (version 4.8.1)[113,114] in R v4.3.0[101] with the
838 biological process ontology, miGSSize of 100, maxGSSize of 500, and an adjusted p-
839 value cut-off of 0.05. The loadings for each gene on the respective principal component
840 were used as input for the GSEA.
841
842 Inferring the direction of exon inclusion
843 We leveraged the NPC and neuron RNA-sequencing data from Liu et al.[29] to assess
844 whether Rbfox2-OE is related to a mature (neuronal) or immature (NPC-specific)
845 splicing pattern. By intersecting our significant alternative splicing results with the Liu
846 et al. data set[43], we assigned the *Rbfox2*-OE splicing events to three categories: 1)
847 Neuronal direction when the exon inclusion level of the respective gene was
848 significantly higher in neurons than in NPCs in the Liu et al. data; 2) NPC direction
849 when the inclusion level was significantly lower in neurons than in NPC; 3) non-
850 regulated, when the inclusion level was not significantly altered, or the splicing event
851 was not detected in the Liu et al. data set[43]. The results of this analysis were visualized
852 with a chord diagram using the circlize package (version 0.4.15)[115] in R v4.3.0[101].
853
854 Motif enrichment analysis
855 We performed a *de novo* motif enrichment analysis to identify enriched motifs in the
856 intronic regions located upstream and downstream of alternatively spliced exons. The
857 intronic sequences around alternatively spliced exons (enriched and suppressed
858 exons separately) and a set of background sequences that were not alternatively
859 spliced (FDR > 0.8 and |ΔPSI| < 0.1) were loaded from the mm39 reference genome
860 (Gencode released 19.10.2022) using pysam (version 0.21)[116].
861 All possible pentameric sequences and their occurrence in the up- and downstream
862 intronic sequences were counted in a sliding window of 50 nt. For each motif, we then
863 subtracted its occurrence in the respective background sequences. Next, motif
864 frequencies were transformed to z-scores using scipy (version 1.10.1)[109]. A motif was
865 considered to be enriched when it had a z-score > 4 ($p < 0.0001$, two-sided z-test).
866 The iClip peaks were used to validate these predicted motifs. We again screened for
867 the occurrence of every possible pentameric sequence within the peaks of RBFOX2
868 and the control, subsequently subtracted the respective values, and performed z-
869 scoring. Next, the z-scores of the iClip and RNA-Sequencing motif enrichment analysis
870 were correlated using scipy (version 1.10.1)[109].
871
872 Motif co-occurrence analysis
873 The co-occurrence of motifs was analyzed similarly to the motif enrichment analysis.
874 400 nt of intronic sequence flanking the alternatively spliced exon or the exon itself
875 was loaded with pysam (version 0.21.0)[116] and screened for the presence of a PTBP-
876 associated CU-rich motifs (UCUCU, UUUCU, UCUUU, CUCUC, UCUCC, CUCUU,
877 UUCCU)[117] with a z-score > 4 upstream and RBFOX2 canonical motif downstream
878 (GCAUG, UGCAU, CAUGC). Moreover, we integrated confirmed binding sites from
879 the iClip data for RBFOX2[52], PTBP1[40], and PTBP2[40]. We visualized this using an
880 UpSet plot (version 0.9.0)[108] using Python (version 3.10.12)[105]. and only included
881 overlapping sets with a minimum size of 1.
882 Further, we examined evolutionarily conserved motif occurrences around these exons
883 by filtering for motifs with a phastcons 35-way[118] score > 0.8.

884

885 Motif localization map

886 Next, we mapped the localization of the enriched motifs identified in the previous
887 analysis on the alternatively spliced exon and the flanking exons. To the end, we
888 computed the motif density in a sliding window of 50 bp for all up- and downregulated
889 events and background (non-regulated events). Motif density corresponds to the
890 fraction of the 50 nt sliding window that is covered by the motif. The estimates were
891 corrected by subtracting the background density for each motif. This analysis was
892 limited to 150 nt of exonic and 400 nt of intronic sequences spanning up- and
893 downstream from the intron/exon boundaries.

894

895 STRING network analysis

896 Potential interaction partners of RBFOX2 were identified with STRING using all
897 potential interaction sources (version 12.0 beta)[119] , allowing 20 interacting proteins
898 and showing confidence as edges. Interactions with RBFOX2 with a confidence score
899 higher than 0.7 were considered high-confidence.

900

901 Statistical analysis of immunohistochemistry data

902 Two groups were compared statistically using a t-test or a Wilcoxon test when
903 assumptions of the parametric test were violated, and a data transformation did not
904 improve the model fit. More than two groups were analyzed using one-way or two-way
905 analysis of variance followed by Tukey's post hoc test or post hoc comparison of model
906 means. Data were transformed using a $\log_e$ or an arcsine square root transformation
907 when assumptions of normality and homogeneity of variance were violated. All p-
908 values are two-tailed and a p-value < 0.05 was considered statistically significant.
909 Statistical analysis was performed using R v4.2.2[101] or Python (version 3.10.12)[105]
910 using scipy (version 1.10.1)[109].

911

912 Overlap of alternatively spliced genes with NDD risk genes

913 Alternatively spliced genes were intersected with high-confidence NDD genes from the
914 GeneTrek database v33[33] to calculate the observed overlap. To obtain a null
915 distribution of the expected overlap, 1317 genes (equal to the total number of
916 alternatively spliced genes upon *Rbfox2*-OE) were randomly sampled from the
917 universe of genes with annotated splice events and the overlap with high-confidence
918 NDD genes and the p-value computed (see Monte Carlo Simulation section for details).

919

920 Monte Carlo Simulation

921 Monte Carlo simulations were performed to evaluate the statistical significance of
922 overlaps for various splicing events and genes. In each simulation, a number of genes
923 equal to the observed count of alternatively splicing events (t*Rbfox*-KO and *Ptbp2*-KO)
924 or genes (NDD risk genes) were randomly sampled from the universe of genes or
925 splicing events. The overlap with the gene set of interest (e.g., high-confidence NDD
926 genes) was then calculated. This process was repeated 100,000 times using a seed
927 of 42 to generate a null distribution of expected overlaps. The p-value was calculated
928 as

$$p = 2 * (1 - CDF(zscore))$$

using Python (version 3.10.12)[105], numpy (version 1.23.5)[103], and scipy (version 1.10.1)[109]. CDF corresponds to the cumulative distribution function of the normal distribution.

Data availability

The RNA Sequencing data generated for this study are available on NCBI SRA (Sequence Read Archive) under the accession number PRJNA1013323.

References

1. Breschi, A., Gingeras, T. R. & Guigó, R. Comparative transcriptomics in human and mouse. *Nat Rev Genet* **18**, 425–440 (2017).
2. Yao, Z. *et al.* A taxonomy of transcriptomic cell types across the isocortex and hippocampal formation. *Cell* **184**, 3222-3241.e26 (2021).
3. Jiang, W. & Chen, L. Alternative splicing: Human disease and quantitative analysis from high-throughput sequencing. *Computational and Structural Biotechnology Journal* **19**, 183–195 (2021).
4. Weyn-Vanhentenryck, S. M. *et al.* Precise temporal regulation of alternative splicing during neural development. *Nat Commun* **9**, 2189 (2018).
5. Raj, B. & Blencowe, B. J. Alternative Splicing in the Mammalian Nervous System: Recent Insights into Mechanisms and Functional Roles. *Neuron* **87**, 14–27 (2015).
6. Barbosa-Morais, N. L. *et al.* The Evolutionary Landscape of Alternative Splicing in Vertebrate Species. *Science* **338**, 1587–1593 (2012).
7. Silbereis, J. C., Pochareddy, S., Zhu, Y., Li, M. & Sestan, N. The Cellular and Molecular Landscapes of the Developing Human Central Nervous System. *Neuron* **89**, 248–268 (2016).
8. Zhang, X. *et al.* Cell-Type-Specific Alternative Splicing Governs Cell Fate in the Developing Cerebral Cortex. *Cell* **166**, 1147-1162.e15 (2016).
9. Zhang, M. *et al.* Axonogenesis Is Coordinated by Neuron-Specific Alternative Splicing Programming and Splicing Regulator PTBP2. *Neuron* **101**, 690-706.e10 (2019).
10. Lin, Y.-S. *et al.* Neuronal Splicing Regulator RBFOX3 (NeuN) Regulates Adult Hippocampal Neurogenesis and Synaptogenesis. *PLOS ONE* (2016).
11. Heck, J. *et al.* More than a pore: How voltage-gated calcium channels act on different levels of neuronal communication regulation. *Channels* **15**, 322–338 (2021).
12. Furlanis, E., Traunmüller, L., Fucile, G. & Scheiffele, P. Landscape of ribosome-engaged transcript isoforms reveals extensive neuronal-cell-class-specific alternative splicing programs. *Nat Neurosci* **22**, 1709–1717 (2019).
13. Cai, Y., Yu, X., Hu, S. & Yu, J. A Brief Review on the Mechanisms of miRNA Regulation. *Genomics, Proteomics & Bioinformatics* **7**, 147–154 (2009).

971 14. Diederichs, S. & Haber, D. A. Dual Role for Argonautes in MicroRNA Processing
972 and Posttranscriptional Regulation of MicroRNA Expression. *Cell* **131**, 1097–1108
973 (2007).
974 15. Lee, R. C., Feinbaum, R. L. & Ambros, V. The C. elegans heterochronic gene lin-
975 4 encodes small RNAs with antisense complementarity to lin-14. *Cell* **75**, 843–
976 854 (1993).
977 16. Cho, K. H. T., Xu, B., Blenkiron, C. & Fraser, M. Emerging Roles of miRNAs in
978 Brain Development and Perinatal Brain Injury. *Frontiers in Physiology* **10**, (2019).
979 17. Makeyev, E. V., Zhang, J., Carrasco, M. A. & Maniatis, T. The MicroRNA miR-124
980 Promotes Neuronal Differentiation by Triggering Brain-Specific Alternative Pre-
981 mRNA Splicing. *Mol Cell* **27**, 435–448 (2007).
982 18. Fisher, E. & Feng, J. RNA splicing regulators play critical roles in neurogenesis.
983 *WIREs RNA* **13**, e1728 (2022).
984 19. Bhalla, K. *et al.* The de novo chromosome 16 translocations of two patients with
985 abnormal phenotypes (mental retardation and epilepsy) disrupt the A2BP1 gene.
986 *J Hum Genet* **49**, 308–311 (2004).
987 20. Sebat, J. *et al.* Strong Association of De Novo Copy Number Mutations with
988 Autism. *Science* **316**, 445–449 (2007).
989 21. Homsy, J. *et al.* De novo mutations in congenital heart disease with
990 neurodevelopmental and other congenital anomalies. *Science* **350**, 1262–1266
991 (2015).
992 22. Verma, S. K. *et al.* Rbfox2 function in RNA metabolism is impaired in hypoplastic
993 left heart syndrome patient hearts. *Sci Rep* **6**, 30896 (2016).
994 23. Gehman, L. T. *et al.* The splicing regulator Rbfox2 is required for both cerebellar
995 development and mature motor function. *Genes Dev.* **26**, 445–460 (2012).
996 24. O'Leary, A. *et al.* Behavioural and functional evidence revealing the role of
997 RBFOX1 variation in multiple psychiatric disorders and traits. *Mol Psychiatry* **27**,
998 4464–4473 (2022).
999 25. Vuong, C. K. *et al.* Rbfox1 Regulates Synaptic Transmission through the Inhibitory
1000 Neuron-Specific vSNARE Vamp1. *Neuron* **98**, 127-141.e7 (2018).
1001 26. Wamsley, B. *et al.* Rbfox1 Mediates Cell-type-Specific Splicing in Cortical
1002 Interneurons. *Neuron* **100**, 846-859.e7 (2018).
1003 27. Zhang, C. *et al.* Defining the regulatory network of the tissue-specific splicing
1004 factors Fox-1 and Fox-2. *Genes Dev.* **22**, 2550–2563 (2008).
1005 28. Choi, S. *et al.* Rbfox family proteins make the homo- and hetero-oligomeric
1006 complexes. *Biochemical and Biophysical Research Communications* **495**, 1022–
1007 1027 (2018).
1008 29. Liu, J., Geng, A., Wu, X., Lin, R.-J. & Lu, Q. Alternative RNA Splicing Associated
1009 With Mammalian Neuronal Differentiation. *Cerebral Cortex* **28**, 2810–2816 (2018).
1010 30. Mullen, R. J., Buck, C. R. & Smith, A. M. NeuN, a neuronal specific nuclear protein
1011 in vertebratesxs. *Development* **116**, 201–211 (1992).
1012 31. Gehman, L. T. *et al.* The splicing regulator Rbfox2 is required for both cerebellar
1013 development and mature motor function. *Genes Dev.* **26**, 445–460 (2012).

1014 32. Jacko, M. *et al.* Rbfox Splicing Factors Promote Neuronal Maturation and Axon
1015 Initial Segment Assembly. *Neuron* **97**, 853-868.e6 (2018).
1016 33. Leblond, C. S. *et al.* Operative list of genes associated with autism and
1017 neurodevelopmental disorders based on database review. *Mol Cell Neurosci* **113**,
1018 103623 (2021).
1019 34. Weyn-Vanhentenryck, S. M. *et al.* Precise temporal regulation of alternative
1020 splicing during neural development. *Nat Commun* **9**, 2189 (2018).
1021 35. Leek, J. T. *et al.* Tackling the widespread and critical impact of batch effects in
1022 high-throughput data. *Nat Rev Genet* **11**, 733–739 (2010).
1023 36. Weißbach, S. *et al.* Reliability of genomic variants across different next-generation
1024 sequencing platforms and bioinformatic processing pipelines. *BMC Genomics*
1025 (2021).
1026 37. Qin, Y. *et al.* A recurrent SHANK1 mutation implicated in autism spectrum disorder
1027 causes autistic-like core behaviors in mice via downregulation of mGluR1-IP3R1-
1028 calcium signaling. *Mol Psychiatry* **27**, 2985–2998 (2022).
1029 38. Schob, C. *et al.* Cognitive impairment and autistic-like behaviour in SAPAP4-
1030 deficient mice. *Transl Psychiatry* **9**, 1–19 (2019).
1031 39. Sanders, B. *et al.* Transcriptional programs regulating neuronal differentiation are
1032 disrupted in DLG2 knockout human embryonic stem cells and enriched for
1033 schizophrenia and related disorders risk variants. *Nat Commun* **13**, 27 (2022).
1034 40. Vuong, J. K. *et al.* PTBP1 and PTBP2 Serve Both Specific and Redundant
1035 Functions in Neuronal Pre-mRNA Splicing. *Cell Reports* **17**, 2766–2775 (2016).
1036 41. Dillon, G. M. *et al.* CLASP2 Links Reelin to the Cytoskeleton during Neocortical
1037 Development. *Neuron* **93**, 1344-1358.e5 (2017).
1038 42. Weißbach, S. *et al.* Cortexa: a comprehensive resource for studying gene
1039 expression and alternative splicing in the murine brain. *BMC Bioinformatics* **25**,
1040 293 (2024).
1041 43. Liu, J., Geng, A., Wu, X., Lin, R.-J. & Lu, Q. Alternative RNA Splicing Associated
1042 With Mammalian Neuronal Differentiation. *Cerebral Cortex* **28**, 2810–2816 (2018).
1043 44. Tissir, F. & Goffinet, A. M. Reelin and brain development. *Nat Rev Neurosci* **4**,
1044 496–505 (2003).
1045 45. Gallo, C. M., Ho, A. & Beffert, U. ApoER2: Functional Tuning Through Splicing.
1046 *Frontiers in Molecular Neuroscience* **13**, (2020).
1047 46. Reddy, S. S., Connor, T. E., Weeber, E. J. & Rebeck, W. Similarities and
1048 differences in structure, expression, and functions of VLDLR and ApoER2.
1049 *Molecular Neurodegeneration* **6**, 30 (2011).
1050 47. Yano, M., Hayakawa-Yano, Y., Mele, A. & Darnell, R. B. Nova2 Regulates
1051 Neuronal Migration through an RNA Switch in Disabled-1 Signaling. *Neuron* **66**,
1052 848–858 (2010).
1053 48. Saito, Y. *et al.* Differential NOVA2-Mediated Splicing in Excitatory and Inhibitory
1054 Neurons Regulates Cortical Development and Cerebellar Function: Neuron.
1055 *Neuron* **101**, 707-720.E5 (2019).

1056 49. Weyn-Vanhentenryck, S. M. *et al.* HITS-CLIP and Integrative Modeling Define the
1057 Rbfox Splicing-Regulatory Network Linked to Brain Development and Autism. *Cell*
1058 *Reports* **6**, 1139–1152 (2014).
1059 50. Yeo, G. W. *et al.* An RNA code for the FOX2 splicing regulator revealed by
1060 mapping RNA-protein interactions in stem cells. *Nat Struct Mol Biol* **16**, 130–137
1061 (2009).
1062 51. Zhang, C. *et al.* Defining the regulatory network of the tissue-specific splicing
1063 factors Fox-1 and Fox-2. *Genes Dev.* **22**, 2550–2563 (2008).
1064 52. Jangi, M., Boutz, P. L., Paul, P. & Sharp, P. A. Rbfox2 controls autoregulation in
1065 RNA-binding protein networks. *Genes Dev.* **28**, 637–651 (2014).
1066 53. Castle, J. C. *et al.* Expression of 24,426 human alternative splicing events and
1067 predicted cis regulation in 48 tissues and cell lines. *Nat Genet* **40**, 1416–1425
1068 (2008).
1069 54. Venables, J. P. *et al.* MBNL1 and RBFOX2 cooperate to establish a splicing
1070 programme involved in pluripotent stem cell differentiation. *Nat Commun* **4**, 2480
1071 (2013).
1072 55. Venables, J. P. *et al.* RBFOX2 Is an Important Regulator of Mesenchymal Tissue-
1073 Specific Splicing in both Normal and Cancer Tissues. *Mol Cell Biol* **33**, 396–405
1074 (2013).
1075 56. Keppetipola, N., Sharma, S., Li, Q. & Black, D. L. Neuronal regulation of pre-
1076 mRNA splicing by polypyrimidine tract binding proteins, PTBP1 and PTBP2. *Crit*
1077 *Rev Biochem Mol Biol* **47**, 360–378 (2012).
1078 57. Ling, J. P. *et al.* PTBP1 and PTBP2 Repress Nonconserved Cryptic Exons. *Cell*
1079 *Reports* **17**, 104–113 (2016).
1080 58. Li, Y. I., Sanchez-Pulido, L., Haerty, W. & Ponting, C. P. RBFOX and PTBP1
1081 proteins regulate the alternative splicing of micro-exons in human brain
1082 transcripts. *Genome Res* **25**, 1–13 (2015).
1083 59. Underwood, J. G., Boutz, P. L., Dougherty, J. D., Stoilov, P. & Black, D. L.
1084 Homologues of the Caenorhabditis elegans Fox-1 Protein Are Neuronal Splicing
1085 Regulators in Mammals. *Molecular and Cellular Biology* **25**, 10005 (2005).
1086 60. Jin, Y. *et al.* A vertebrate RNA-binding protein Fox-1 regulates tissue-specific
1087 splicing via the pentanucleotide GCAUG. *The EMBO Journal* **22**, 905–912 (2003).
1088 61. Bak, M. *et al.* MAPP unravels frequent co-regulation of splicing and
1089 polyadenylation by RNA-binding proteins and their dysregulation in cancer. *Nat*
1090 *Commun* **15**, 4110 (2024).
1091 62. Huang, R. *et al.* NCAM regulates temporal specification of neural progenitor cells
1092 via profilin2 during corticogenesis. *Journal of Cell Biology* **219**, e201902164
1093 (2019).
1094 63. Sarkisian, M. R., Bartley, C. M. & Rakic, P. Trouble making the first move:
1095 interpreting arrested neuronal migration in the cerebral cortex. *Trends in*
1096 *Neurosciences* **31**, 54–61 (2008).

1097 64. Licatalosi, D. D. *et al.* Ptbp2 represses adult-specific splicing to regulate the
1098 generation of neuronal precursors in the embryonic brain. *Genes Dev.* **26**, 1626–
1099 1642 (2012).
1100 65. Todorov, H. *et al.* Stage-specific expression patterns and co-targeting
1101 relationships among miRNAs in the developing mouse cerebral cortex. *Commun*
1102 *Biol* **7**, 1–14 (2024).
1103 66. Yang, Y. *et al.* Single-cell long-read sequencing in human cerebral organoids
1104 uncovers cell-type-specific and autism-associated exons. *Cell Reports* **42**, (2023).
1105 67. Chau, K. K. *et al.* Full-length isoform transcriptome of the developing human brain
1106 provides further insights into autism. *Cell Reports* **36**, (2021).
1107 68. Turner, T. N. *et al.* Genome Sequencing of Autism-Affected Families Reveals
1108 Disruption of Putative Noncoding Regulatory DNA. *The American Journal of*
1109 *Human Genetics* **98**, 58–74 (2016).
1110 69. Bacchelli, E. *et al.* An integrated analysis of rare CNV and exome variation in
1111 Autism Spectrum Disorder using the Infinium PsychArray. *Sci Rep* **10**, 3198
1112 (2020).
1113 70. Griswold, A. J. *et al.* Targeted massively parallel sequencing of autism spectrum
1114 disorder-associated genes in a case control cohort reveals rare loss-of-function
1115 risk variants. *Molecular Autism* **6**, 43 (2015).
1116 71. Kanduri, C. *et al.* The landscape of copy number variations in Finnish families with
1117 autism spectrum disorders. *Autism Research* **9**, 9–16 (2016).
1118 72. Fanciulli, M. *et al.* Copy number variations and susceptibility to lateral temporal
1119 epilepsy: A study of 21 pedigrees. *Epilepsia* **55**, 1651–1658 (2014).
1120 73. Lal, D. *et al.* Rare exonic deletions of the RBFOX1 gene increase risk of idiopathic
1121 generalized epilepsy. *Epilepsia* **54**, 265–271 (2013).
1122 74. Lal, D. *et al.* Extending the phenotypic spectrum of RBFOX1 deletions: Sporadic
1123 focal epilepsy. *Epilepsia* **56**, e129–e133 (2015).
1124 75. Gehman, L. T. *et al.* The splicing regulator Rbfox1 (A2BP1) controls neuronal
1125 excitation in the mammalian brain. *Nat Genet* **43**, 706–711 (2011).
1126 76. Wen, M. *et al.* Upregulation of RBFOX1 in the malformed cortex of patients with
1127 intractable epilepsy and in cultured rat neurons. *International Journal of Molecular*
1128 *Medicine* **35**, 597–606 (2015).
1129 77. Chung, Y. *et al.* Altered Rbfox1-Vamp1 pathway and prefrontal cortical
1130 dysfunction in schizophrenia. *Mol Psychiatry* 1–10 (2024) doi:10.1038/s41380-
1131 024-02417-8.
1132 78. Conboy, J. G. Developmental regulation of RNA processing by Rbfox proteins.
1133 *WIREs RNA* **8**, e1398 (2017).
1134 79. Mukherjee, A. & Nongthomba, U. To RNA-binding and beyond: Emerging facets
1135 of the role of Rbfox proteins in development and disease. *WIREs RNA* **15**, e1813
1136 (2023).
1137 80. Cayouette, M. & Raff, M. Asymmetric segregation of Numb: a mechanism for
1138 neural specification from Drosophila to mammals. *Nat Neurosci* **5**, 1265–1269
1139 (2002).

1140 81. Gulino, A., Di Marcotullio, L. & Screpanti, I. The multiple functions of Numb.
1141 *Experimental Cell Research* **316**, 900–906 (2010).
1142 82. Keppetipola, N. M. *et al.* Multiple determinants of splicing repression activity in the
1143 polypyrimidine tract binding proteins, PTBP1 and PTBP2. *RNA* **22**, 1172–1180
1144 (2016).
1145 83. Linares, A. J. *et al.* The splicing regulator PTBP1 controls the activity of the
1146 transcription factor Pbx1 during neuronal differentiation. *eLife* **4**, e09268 (2015).
1147 84. Uhlén, M. *et al.* Tissue-based map of the human proteome. *Science* **347**, 1260419
1148 (2015).
1149 85. Ellis, J. A., Hale, M. A., Cleary, J. D., Wang, E. T. & Andrew Berglund, J.
1150 Alternative Splicing Outcomes Across an RNA-Binding Protein Concentration
1151 Gradient. *Journal of Molecular Biology* **435**, 168156 (2023).
1152 86. Begg, B. E., Jens, M., Wang, P. Y., Minor, C. M. & Burge, C. B. Concentration-
1153 dependent splicing is enabled by Rbfox motifs of intermediate affinity. *Nat Struct*
1154 *Mol Biol* **27**, 901–912 (2020).
1155 87. Dredge, B. K. & Jensen, K. B. NeuN/Rbfox3 Nuclear and Cytoplasmic Isoforms
1156 Differentially Regulate Alternative Splicing and Nonsense-Mediated Decay of
1157 Rbfox2. *PLOS ONE* **6**, e21585 (2011).
1158 88. Damianov, A. & Black, D. L. Autoregulation of Fox protein expression to produce
1159 dominant negative splicing factors. *RNA* **16**, 405–416 (2010).
1160 89. Nowakowski, T. J. *et al.* Regulation of cell-type-specific transcriptomes by
1161 microRNA networks during human brain development. *Nat Neurosci* **21**, 1784–
1162 1792 (2018).
1163 90. Florio, M. *et al.* Human-specific gene ARHGAP11B promotes basal progenitor
1164 amplification and neocortex expansion. *Science* **347**, 1465–1470 (2015).
1165 91. Ma, J. *et al.* Identification of miR-22-3p, miR-92a-3p, and miR-137 in peripheral
1166 blood as biomarker for schizophrenia. *Psychiatry Research* **265**, 70–76 (2018).
1167 92. Shi, W. *et al.* Aberrant expression of serum miRNAs in schizophrenia. *Journal of*
1168 *Psychiatric Research* **46**, 198–204 (2012).
1169 93. Talebizadeh, Z., Butler, M. G. & Theodoro, M. F. Feasibility and relevance of
1170 examining lymphoblastoid cell lines to study role of microRNAs in autism. *Autism*
1171 *Research* **1**, 240–250 (2008).
1172 94. Huang, F. *et al.* Investigation of Gene Regulatory Networks Associated with
1173 Autism Spectrum Disorder Based on MiRNA Expression in China. *PLOS ONE* **10**,
1174 e0129052 (2015).
1175 95. Basak, O. & Taylor, V. Identification of self-replicating multipotent progenitors in
1176 the embryonic nervous system by high Notch activity and Hes5 expression.
1177 *European Journal of Neuroscience* **25**, 1006–1022 (2007).
1178 96. Schindelin, J. *et al.* Fiji: an open-source platform for biological-image analysis. *Nat*
1179 *Methods* **9**, 676–682 (2012).
1180 97. BBMap. *SourceForge* https://sourceforge.net/projects/bbmap/ (2022).
1181 98. Dobin, A. *et al.* STAR: ultrafast universal RNA-seq aligner. *Bioinformatics* **29**, 15–
1182 21 (2013).

99. Liao, Y., Smyth, G. K. & Shi, W. featureCounts: an efficient general purpose program for assigning sequence reads to genomic features. *Bioinformatics* **30**, 923–930 (2014).
100. Love, M. I., Huber, W. & Anders, S. Moderated estimation of fold change and dispersion for RNA-seq data with DESeq2. *Genome Biology* **15**, 550 (2014).
101. R Core Team. R: A language and environment for statistical computing. R Foundation for Statistical Computing (2022).
102. rMATS: Robust and flexible detection of differential alternative splicing from replicate RNA-Seq data | PNAS. https://www.pnas.org/doi/10.1073/pnas.1419161111.
103. Array programming with NumPy | Nature. https://www.nature.com/articles/s41586-020-2649-2.
104. team, T. pandas development. pandas-dev/pandas: Pandas. Zenodo https://doi.org/10.5281/zenodo.8092754 (2023).
105. The Python Language Reference — Python 3.10.12 documentation. https://docs.python.org/3.10/reference/.
106. Matplotlib: A 2D Graphics Environment | IEEE Journals & Magazine | IEEE Xplore. https://ieeexplore.ieee.org/document/4160265.
107. Waskom, M. L. seaborn: statistical data visualization. *Journal of Open Source Software* **6**, 3021 (2021).
108. Lex, A., Gehlenborg, N., Strobelt, H., Vuillemot, R. & Pfister, H. UpSet: Visualization of Intersecting Sets. *IEEE Transactions on Visualization and Computer Graphics* **20**, 1983–1992 (2014).
109. Virtanen, P. *et al.* SciPy 1.0: fundamental algorithms for scientific computing in Python. *Nat Methods* **17**, 261–272 (2020).
110. Smith, T., Heger, A. & Sudbery, I. UMI-tools: modeling sequencing errors in Unique Molecular Identifiers to improve quantification accuracy. *Genome Res.* **27**, 491–499 (2017).
111. Lovci, M. T. *et al.* Rbfox proteins regulate alternative mRNA splicing through evolutionarily conserved RNA bridges. *Nat Struct Mol Biol* **20**, 1434–1442 (2013).
112. Todorov, H., Fournier, D. & Gerber, S. Principal components analysis: theory and application to gene expression data analysis. *Genomics Comput Biol* **4**, 100041 (2018).
113. Wu, T. *et al.* clusterProfiler 4.0: A universal enrichment tool for interpreting omics data. *The Innovation* **2**, 100141 (2021).
114. Yu, Guangchuang, Wang, Li-Gen, & He, Qing-Yu. clusterProfiler: an R Package for Comparing Biological Themes Among Gene Clusters. *OMICS: A Journal of Integrative Biology* **16**, 284–287 (2012).
115. Gu, Z., Gu, L., Eils, R., Schlesner, M. & Brors, B. circlize implements and enhances circular visualization in R. *Bioinformatics* **30**, 2811–2812 (2014).
116. Pysam. pysam-developers (2023).

117. Llorian, M. *et al.* Position-dependent alternative splicing activity revealed by global profiling of alternative splicing events regulated by PTB. *Nature structural & molecular biology* **17**, 1114 (2010).
118. Siepel, A. *et al.* Evolutionarily conserved elements in vertebrate, insect, worm, and yeast genomes. *Genome Res.* **15**, 1034–1050 (2005).
119. Szklarczyk, Damian *et al.* STRING v11: protein–protein association networks with increased coverage, supporting functional discovery in genome-wide experimental datasets. *Nucleic Acids Research* **47**, (2019).

Acknowledgments

S.W acknowledges financial support from the Emergent Algorithmic Intelligence Center of the Johannes Gutenberg University Mainz funded by the Carl-Zeiss-Stiftung. H.T. and S.G. acknowledge financial support from the Landesinitiative Rheinland-Pfalz and the Resilience, Adaptation, and Longevity (ReALity) initiative of the Johannes Gutenberg University of Mainz. J.W. acknowledges funding from the DFG (WI 3837/10-1).

Author information

Contributions

S.W. performed the bioinformatics analyses, interpreted and visualized the results. H.T. contributed to interpreting the results and performed statistical analyses. L.S. performed in-utero electroporation experiments and analyzed the data. L.Z. and S.M. performed immunostainings and analyzed the data. A.S. performed cell culture, RT-qPCR, and Western blot experiments. S.L.Z. performed Luciferase Assays. D.H. performed bioinformatics analyses. T.V. provided the *in vitro* neuronal differentiation model. DS and SS analyzed data and revised the manuscript. M.H. and S.G. provided supervision and organized funding. J.W. designed the research, supervised the study, and organized funding. S.W., H.T., and J.W. wrote the manuscript. All authors read and approved the final version of the manuscript.

Ethics declarations

Ethics approval

All animal experiments were performed in accordance with the regulations of the local authorities (Landesuntersuchungsamt Rheinland-Pfalz, license number 23 177-07/G 13-1-089).

Competing interests

The authors declare no conflict of interest.